https://doi.org/10.5194/egusphere-2026-6328
Preprint. Discussion started: 16 November 2026
© Author(s) 2026. CC BY 4.0 License.

FASTMIP-CMIP7: A Coordinated Multi-Emulator Ensemble for Rapid, Spatially Resolved Climate Projections under CMIP7 Scenarios

Sarah Schöngart[1], Marit Sandstad[2], Christopher B. Womack[1,3], Niklas Schwind[4,5], Maura Dewey[2], Shahine Bouabid[6], Nicolai Meinshausen[7, 12], Verena Kain[4,8], Daniel Hooke[9], Chris Smith[10], Jarmo Kikstra[4], Annika Högner[4,5], Edward Byers[4], Chris D. Jones[9,10], Eleanor Burke[9], Raffaela Langer[4,5], Camilla Mathison[9,11], Yann Quilcaille[1], Benjamin M. Sanderson[2], Carl-Friedrich Schleussner[4,5], Noelle E. Selin[6,3], Michael Windisch[1], and Sonia I. Seneviratne[1]

[1]Institute for Atmospheric and Climate Science, ETH Zürich, Zürich, Switzerland
[2]CICERO International Center for Climate Research, Oslo, Norway
[3]Center for Sustainability Science and Strategy, Massachusetts Institute of Technology, Cambridge, MA, USA
[4]International Institute for Applied Systems Analysis (IIASA), Laxenburg, Austria
[5]Geography Department, Humboldt-Universität zu Berlin, Berlin, Germany
[6]Department of Earth, Atmospheric and Planetary Sciences, Massachusetts Institute of Technology, Cambridge, MA, USA
[7]School of Geography, Earth and Atmospheric Sciences, The University of Melbourne, Melbourne, Australia
[8]CERN, European Organization for Nuclear Research, Geneva, Switzerland
[9]Met Office Hadley Centre, Exeter, UK
[10]School of Geographical Sciences, University of Bristol, Bristol, UK
[11]University of Leeds, Leeds, UK
[12]Department of Statistics, University of Washington, Washington, USA

Correspondence: Sarah Schöngart (sarah.schoengart@env.ethz.ch)

Abstract. Earth System Models (ESMs) remain the gold standard for translating socioeconomic scenarios into spatially resolved climate projections, but their computational cost limits the number of scenarios and ensemble members that can be simulated and ties projections to the evidence available when simulations are performed. Climate emulators, which are statistical and machine-learning models trained on ESM output, enable large ensembles and allow projections to be updated as new observations emerge. Here, we present FASTMIP-CMIP7, a coordinated ensemble of seven emulators providing spatially and temporally resolved projections of temperature, precipitation and climate impact indicators for four newly released CMIP7 scenarios, spanning very low (VL) to high (H) emissions. Despite scenario ranges having narrowed in CMIP7 comapred to CMIP6, emissions pathways remain the dominant source of uncertainty in regional end-of-century temperature projections, making mitigation the strongest lever for limiting future warming. In 2100, global land temperature reaches 2.3 °C under stringent mitigation (VL), and 3.9 °C under the current-policies scenario (M), approximately 1.4 times the global mean warming. Under M, even the coolest 5% of years in 2100 are warmer over land than 95% of present-day years. Precipitation projections are more heterogeneous, with internal variability and regional climate responses often obscuring scenario differences. Nevertheless, robust drying emerges in Northern South America and the Mediterranean, where additional drying relative to today is 2.5 to almost four times greater under current policies (M) than under stringent mitigation (VL). Structural differences between

https://doi.org/10.5194/egusphere-2026-6328
Preprint. Discussion started: 16 November 2026
© Author(s) 2026. CC BY 4.0 License.

emulators and choices in training, testing and validation introduce a new layer of uncertainty to emulated ensembles. Common, streamlined validation experiments are needed to establish confidence in emulated projections and support the broader integration of climate emulators into future climate assessments.

1 Introduction

Climate change affects decision-making across scales, with today's policy and socioeconomic choices shaping the future that will materialise. These choices are encoded in future scenarios, which consist of internally consistent narratives of socioeconomic development, translated into emission and land-use trajectories by Integrated Assessment Models (IAMs) (O'Neill et al., 2016; Van Vuuren et al., 2026). Earth System Models (ESMs) then translate these trajectories into physical climate outcomes (Tebaldi et al., 2021), and sectoral impact models (IMs) resolve their consequences for human and natural systems (Frieler et al., 2025). The resulting information underpins international agreements such as the Paris Agreement (UNFCCC), informs adaptation planners and central banks, and feeds into assessments by the Intergovernmental Panel on Climate Change (IPCC) (IPCC, 2022). The Scenario Model Intercomparison Project for the seventh phase of the Coupled Model Intercomparison Project (ScenarioMIP-CMIP7; Dunne et al., 2025) has recently released a new generation of these pathways (Van Vuuren et al., 2026), starting the next cycle of translating them into spatially resolved climate information.

Traditionally, this translation step relies on ESMs, which resolve the underlying physical, chemical and biological processes explicitly but at a high computational cost: producing the CMIP6 data required more than a billion core hours and generated about 40 PB of output (Acosta et al., 2024). Beyond greenhouse gas emissions, ESMs require spatially explicit scenario inputs, such as gridded aerosol emissions and land-use change. Most IAMs do not provide these directly, so they have to be derived through additional harmonisation and downscaling steps that require specialised expertise (Chini et al., 2021). The simulations themselves, and the processing of their output for publication, take weeks to months for a single ESM. As a result, there is a delay between the release of new scenarios and the availability of spatially resolved climate data for downstream applications, and the number of scenarios and ensemble members that can be simulated is limited. This affects what assessments such as the IPCC Assessment Reports (AR) can draw on within their timelines. In AR6, Working Group I assessed five core SSP scenarios (Lee et al., 2021), whereas Working Group III assessed about 1,200 scenarios (Riahi et al., 2022; Byers et al., 2022), and Working Group II impact assessments drew largely on literature based on earlier CMIP generations (Rawshan Ara Begum et al., 2022; Pirani et al., 2024).

Spatially explicit emulators offer a way to close this gap (Tebaldi et al., 2025). They trade mechanistic realism for computational efficiency, which suits decision contexts where quantifying probabilities and risks matters more than resolving the underlying physical drivers. Emulators are increasingly gaining a formal role in the climate assessment pipeline, including in emerging AR7 workflows (Intergovernmental Panel on Climate Change, 2025).

Here, we present FASTMIP-CMIP7, the second phase of the Fast Assessment for Scenario Trajectories Multi-emulator Intercomparison Project (FASTMIP), and show how coordinated multi-emulator ensembles can deliver spatially explicit climate projections for the CMIP7 scenarios shortly after their release. We apply seven emulators, GCMagicc (Meinshausen et al.,

https://doi.org/10.5194/egusphere-2026-6328
Preprint. Discussion started: 16 November 2026
© Author(s) 2026. CC BY 4.0 License.

2026a), MESMER (Beusch et al., 2020b; Bauer et al., 2026), METEOR (Sandstad et al., 2025; Sanderson et al., 2026b), MIT-EarthSampler (Bouabid et al., 2026), PRIME (Mathison et al., 2025), RIME-X (Byers et al., 2025; Schwind et al., 2026a) and SCALES (Kain et al., 2026), to four CMIP7 scenarios spanning very low to high emissions. All emulators are trained on CMIP6 ESM output and run under a common protocol and forcing. For emulators driven by global concentrations, radiative forcing or temperature, these inputs are derived from emissions with the simple climate model (SCM) FaIR v2.2.4 and parameter set v1.6.0 (Leach et al., 2021; Smith et al., 2024; Smith, 2026). This set-up allows us to generate large ensembles and to decompose the resulting uncertainty into contributions from scenario choice, the global response, the regional response and internal variability. FASTMIP-CMIP7 scales up from a three-emulator proof of concept for CMIP6 scenarios (Windisch et al., 2026) to a seven-emulator intercomparison for the new CMIP7 scenarios, and establishes a blueprint for delivering coordinated regional climate information at the start of an assessment cycle.

The remainder of the paper is structured as follows. Section 2 summarises the experiment design. Section 3 gives an overview of the generated data and the advantages of large ensembles. Section 4 presents CMIP7-specific results, including the uncertainty decomposition, and Section 5 compares estimates across emulators. We discuss our findings in Section 7 and describe our methods in Section 6, with additional technical information in the Supplement.

2 Experiment design

FASTMIP-CMIP7 generates spatially explicit climate projections for four CMIP7 scenarios with seven CMIP6-trained emulators: GCMagicc, MESMER, METEOR, MIT-EarthSampler, PRIME, RIME-X and SCALES (Fig. 1). The experiment is designed as a conditional global-to-local translation experiment. Emission scenarios are first translated into an observationally constrained ensemble of global climate variables, such as global mean surface-air temperature (GSAT) and effective radiative forcing. The emulators then translate these global trajectories into regional climate fields. This design treats the global and regional climate responses as approximately separable components of uncertainty and samples them independently (Beusch et al., 2020b, a; Swaminathan et al., 2024). As a result, it also covers combinations of global properties (e.g. climate sensitivity) and regional patterns that are absent from the CMIP6 ensemble, extending the CMIP "ensemble of opportunity" (Tebaldi and Knutti, 2007) beyond the scenario–ESM combinations that have been simulated. FASTMIP-CMIP7 is therefore not intended as a one-to-one reconstruction of how individual CMIP6 ESMs would respond to the CMIP7 scenarios.

2.1 Scenarios

We consider four CMIP7 scenarios spanning a wide range of emissions and warming: Very Low (VL), Low (L), Medium (M) and High (H) (Van Vuuren et al., 2026). VL represents the lowest warming considered plausible given feasibility constraints and follows a peak-and-decline trajectory, reaching a median warming of 1.6 °C (5–95 %: 1.1–2.6 °C) in 2100 relative to 1850–1900. L reaches 1.8 °C (1.3–2.7 °C). M extends current policies and trends and reaches 2.9 °C (2.2–4.0 °C), while H represents emissions at the high end of what is considered plausible, including a rollback of current mitigation policies, and reaches 3.3 °C (2.6–4.5 °C) (Fig. 1b).

https://doi.org/10.5194/egusphere-2026-6328
Preprint. Discussion started: 16 November 2026
© Author(s) 2026. CC BY 4.0 License.

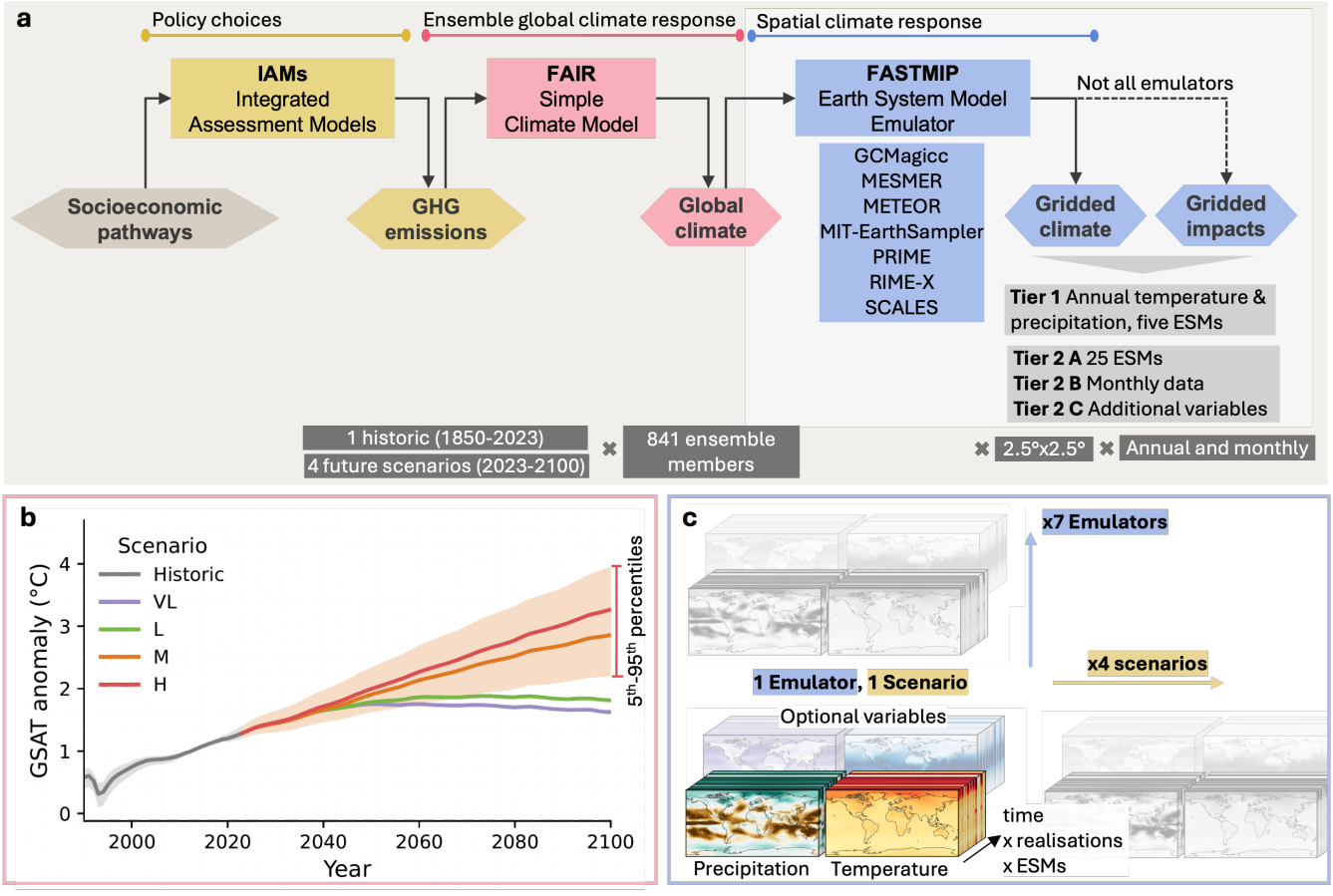


Figure 1. FASTMIP-CMIP7 workflow and experiment design. a, Socioeconomic pathways are translated into emission trajectories by IAMs, which the SCM FaIR converts into an 841-member ensemble of global climate variables for the historical period (1850–2023) and four CMIP7 scenarios (2024–2100). Seven emulators translate these global trajectories into gridded climate fields at 2.5° × 2.5° and annual or monthly resolution, and some emulators additionally provide gridded impact indicators. Tier 1 covers annual temperature and precipitation for five ESMs; Tier 2 extends this to 25 ESMs (2A), monthly data (2B) and additional variables (2C). **b**, Global mean surface air temperature (GSAT) anomaly relative to 1850–1900 from the FaIR ensemble for the historical period and the four scenarios. Lines show the median, and shading the 5–95 % range only for H. **c**, Schematic of the dimensions of the resulting emulated dataset: emulators × scenarios × variables × ESMs × realisations × space × time.

https://doi.org/10.5194/egusphere-2026-6328
Preprint. Discussion started: 16 November 2026
© Author(s) 2026. CC BY 4.0 License.

2.2 Global climate response

Global climate trajectories are provided by FaIR v2.2.4 with calibration v1.6.0 (Leach et al., 2021; Smith et al., 2024; Smith, 2026), which supplies 841 ensemble members per scenario, including GSAT, greenhouse gas and aerosol concentrations and effective radiative forcing. Each modelling team either uses the full ensemble or a subsample that keeps the sample size tractable while representing the full uncertainty range (Schwaab et al., 2024).

2.3 Regional climate response

The emulators translate the global trajectories into gridded climate fields on a common $2.5° \times 2.5°$ grid. All emulators are trained on CMIP6 output from up to 25 ESMs (Table S3). GCMagicc, MESMER, METEOR, MIT-EarthSampler and PRIME apply ESM-specific global-to-regional translations, whereas RIME-X directly produces a multi-ESM distribution by resampling the CMIP6 archive, and SCALES estimates distribution parameters rather than generating individual realisations. All emulators except PRIME include internal variability. Combining FaIR ensemble members with their own internal-variability generation, the emulators provide between 100 and 1,000 realisations per ESM and scenario (Sect. 3).

2.4 Protocol and outputs

The protocol is tiered by ESMs, temporal resolution and variables (Fig. 1a). Tier 1 covers annual near-surface air temperature and precipitation for five ESMs: ACCESS-ESM1-5 (Ziehn et al., 2019), CanESM5 (Swart et al., 2019), IPSL-CM6A-LR (Boucher et al., 2019), MIROC6 (Tatebe and Watanabe, 2018) and MPI-ESM1-2-LR (Schupfner et al., 2021). These were chosen for their large training ensembles and to span a range of transient climate responses to cumulative emissions (TCRE). Tier 2 extends the protocol to 25 ESMs (Tier 2A), monthly resolution (Tier 2B) and additional variables (Tier 2C), including soil moisture, humidity, wind, radiative fluxes, crop yields and impact indicators such as heat, drought and fire-weather metrics. All projections cover 1850–2100, with the historical period ending in 2023 and the scenarios starting in 2024. Temperature is provided as an anomaly relative to 1850–1900, and precipitation as a log-ratio relative to its 1850–1900 climatology, which we convert to percentage change for presentation.

2.5 Uncertainty and applications

The ensemble allows uncertainty to be attributed to scenario choice, the global climate response, the regional response and internal variability, with socioeconomic uncertainty additionally included for selected impact variables. The resulting data support spatial climate indicators and downstream applications that link climate outcomes to socioeconomic assumptions, such as lifetime heat exposure or drought.

https://doi.org/10.5194/egusphere-2026-6328
Preprint. Discussion started: 16 November 2026
© Author(s) 2026. CC BY 4.0 License.

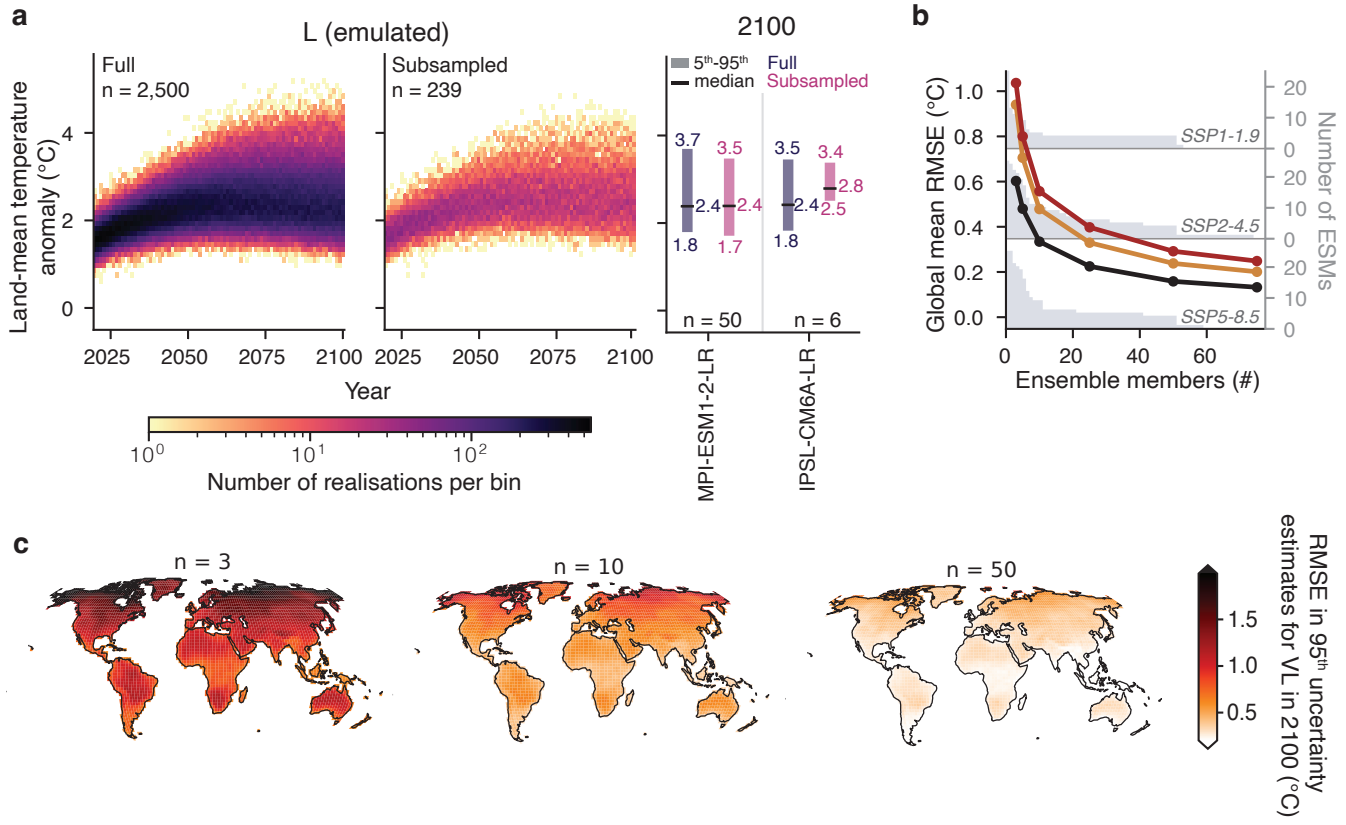


Figure 2. Effect of ensemble size on uncertainty estimates: FASTMIP versus CMIP6 availability. a, Annual land-mean surface air temperature anomaly under the Low (L) scenario emulated with MESMER (Beusch et al., 2020a), shown as 2D histograms (colour: number of realisations per bin, log scale). Left: full emulated ensemble of 25 ESMs × 100 realisations ($n = 2{,}500$). Middle: the same ensemble subsampled to match the number of realisations per ESM available for SSP1-1.9 in CMIP6 (Brunner et al., 2020) ($n = 239$). Right: median (black line) and 5th–95th percentile range (bars) of GSAT in 2100 for two example ESMs, MPI-ESM1-2-LR and IPSL-CM6A-LR, from the full ensemble ($n = 100$, dark blue) and the subsampled ensemble ($n = 50$ and $n = 6$, respectively; pink). **b**, Global mean of local errors in the median (black), 5th (orange) and 95th (red) percentile estimates of local temperature anomaly for L in 2100, as a function of ensemble size. For each ensemble size, we drew 500 bootstrap subsamples from the 100-member emulated ensemble of each ESM and computed, at every grid point, the root-mean-square error (RMSE) of each percentile relative to the full ensemble. We then averaged these local RMSEs area-weighted over the globe and across ESMs. Grey shading (right axis) shows how many of the 25 ESMs provide at least a given number of ensemble members in CMIP6 for SSP1-1.9 (top), SSP2-4.5 (middle) and SSP5-8.5 (bottom). **c**, Spatial distribution of the RMSE in the 95th-percentile estimate for L in 2100, computed as in **b** and averaged across ESMs, for ensemble sizes of 3 (left), 10 (middle) and 50 (right).

https://doi.org/10.5194/egusphere-2026-6328
Preprint. Discussion started: 16 November 2026
© Author(s) 2026. CC BY 4.0 License.

3 Emulating large ensembles

Large ensembles are needed to separate forced change from internal variability and to sample extremes, but in CMIP6, ensemble sizes were limited by computational cost and storage (Acosta et al., 2024), and availability was uneven across ESMs and scenarios (Table S1). For SSP1-1.9, a total of 239 realisations were generated across the 25 Tier 2A ESMs considered. However, only 13 of these 25 ESMs provided any realisations, while four ESMs (EC-Earth3, CanESM5, MIROC6 and MPI-ESM1-2-LR) contributed (85 %) of all realisations (i.e., 202 of 239), and the median contributing ESM provided five (Fig. 2a, middle; Fig. 2b, grey shading). Coverage is higher for more widely run scenarios: all 25 ESMs provide at least one realisation for SSP5-8.5, but only nine provide ten or more.

Emulators, in contrast, can generate large ensembles at negligible inference cost, allowing scenario spaces to be explored in more detail than with ESMs alone. Within FASTMIP, MESMER provides 100 realisations per scenario and ESM, GCMagicc and METEOR 200 each, PRIME 841, and the MIT-EarthSampler 1,000; PRIME's realisations, however, do not include internal variability. Two emulators take a different approach. RIME-X resamples outcome distributions from the CMIP6 archive, so its effective sample size is set by the available data, and SCALES estimates distribution parameters directly rather than generating realisations. These ensemble sizes and approaches were chosen by the modelling teams, and the practical limit is storage and post-processing rather than inference time. For any given scenario, MESMER alone thus provides 2,500 realisations across the 25 Tier 2A ESMs (Fig. 2a, left).

To quantify what larger ensembles gain, we subsampled the MESMER ensemble of each ESM for L to between 3 and 75 of its 100 realisations (500 bootstrap draws each) and compared the estimated 5th, 50th and 95th percentiles of local annual temperature in 2100 with those of the full ensemble (Fig. 2b). Averaged over the globe, the local sampling error decreases roughly with $1/\sqrt{n}$, where n is the ensemble size, and the tails converge more slowly than the median. The RMSE of the 95th percentile falls from about 1.04 °C at $n = 3$ to 0.25 °C at $n = 75$, compared with 0.60 to 0.13 °C for the median; values for $n > 50$ are likely biased because subsamples share many members with the reference (Milinski et al., 2020). Most CMIP6 ESMs sit on the steep part of these curves (Fig. 2b, grey shading). The errors are largest over northern mid- and high-latitude land, where interannual variability is high (Fig. 2c). Within a specific subsample, the error strongly depends on the drawn realisations, we illustratively highlight a single subsampled drawing in Fig. 2a (right) where the six realisations available for IPSL-CM6A-LR under SSP1-1.9, narrow the 5th–95th percentile range of GSAT in 2100 from 1.8–3.5 °C to 2.5–3.4 °C.

How large an ensemble needs to be depends on the application, in particular on the studied quantity and the acceptable error. About five to ten members suffice to estimate the global-mean warming trend, whereas regional temperature over high-latitude land, tropical precipitation and changes in internal variability can require 50 to more than 100 (Milinski et al., 2020). Adaptation decisions, however, often depend on extremes rather than central estimates (Mankin et al., 2020; Deser et al., 2020). Design standards typically target events with annual exceedance probabilities of 1 % to 0.1 %, such as 100-year flood zones or the 1,000-year scenario of the EU Floods Directive (European Union, 2007). Estimating such events robustly requires on the order of 10^3 to 10^4 independent annual samples (Thompson et al., 2017). Emulators bring ensembles of this size within reach across scenarios and ESMs.

https://doi.org/10.5194/egusphere-2026-6328
Preprint. Discussion started: 16 November 2026
© Author(s) 2026. CC BY 4.0 License.



However, the errors in Fig. 2 measure sampling error relative to the emulator's own distribution. Whether that distribution is correct in the tails ultimately determines the added value of emulated large ensembles. This depends on whether emulators are explicitly trained and tested for extremes, on how many ESM realisations are available for validation, and on the emulator formulation. We return to these considerations in the Discussion (Section 7).

4 Temperature and precipitation ensembles for CMIP7

Global results are derived directly from the 841-member FaIR ensemble, whereas all gridded and regional results are based on emulated data. We focus on Tier 1 data, i.e. annual temperature and precipitation emulated for the five Tier 1 ESMs (Table S3). Unless stated otherwise, we report the multi-emulator mean of the emulated mean, 5th and 95th percentiles of the multi-ESM distribution, either per grid cell or aggregated to AR6 land regions (Iturbide et al.).

GSAT in the FaIR ensemble 2100 reaches 1.6 °C (1.1–2.6 °C) under VL, 1.8 °C (1.3–2.7 °C) under L, 2.9 °C (2.2–4.0 °C) under M and 3.3 °C (2.6–4.5 °C) under H, relative to 1850–1900 (Fig. 1). With about 1.3 °C of warming reached by 2023, this corresponds to an additional 0.3, 0.5, 1.6 and 2.0 °C, respectively. Current policies (M) are thus on track to cause about five times as much additional warming relative to present-day as stringent mitigation (VL).

4.1 Sources of uncertainty

Large ensembles make it possible to decompose the projected ensemble spread into contributions from scenario choice, the global temperature response, the multi-ESM regional response and internal variability. Five emulator groups performed this partitioning with a nested analysis of variance (Figs. 4 and 5; Methods). This decomposition is scale dependent: internal variability gains weight at finer spatial and temporal resolution, whereas scenario uncertainty gains weight for aggregates such as regional or global land means (Lehner et al.).

For temperature, scenario choice is the largest source of uncertainty in 2100 across regions and emulators, followed by the global temperature response (Fig. 4). These values shift over time: In 2025, internal variability is the largest source of uncertainty across all emulators in Northern South-America while regional response uncertainty dominates for MESMER, METEOR and MIT-EarthSampler in Western-Africa. Across regions, scenario uncertainty gains importance over time as the emission pathways start to diverge. Mitigation is therefore the largest lever on end-of-century regional warming. The absolute contribution of internal variability is highest in northern latitudes and lowest over Southeast Asia, and differs between emulators (see Sect. 7 for a discussion).

The second-largest source of uncertainty in 2100, the global temperature response, is set by the calibration of the SCM, here FaIR (Smith, 2026), and this calibration is itself evolving with new observations. After removing internal variability from recent temperature trends and adding trends in Earth's energy imbalance, Gyuleva et al. (2026) find that observations over 2001–2025 support a higher transient climate response than earlier temperature-based constraints, suggesting that high-sensitivity ESMs may be less implausible than previously assessed. Other updates that include the record years 2023 and 2024 find values close to earlier assessments (Boardman et al., 2026). Because emulators separate the global response from its

https://doi.org/10.5194/egusphere-2026-6328
Preprint. Discussion started: 16 November 2026
© Author(s) 2026. CC BY 4.0 License.

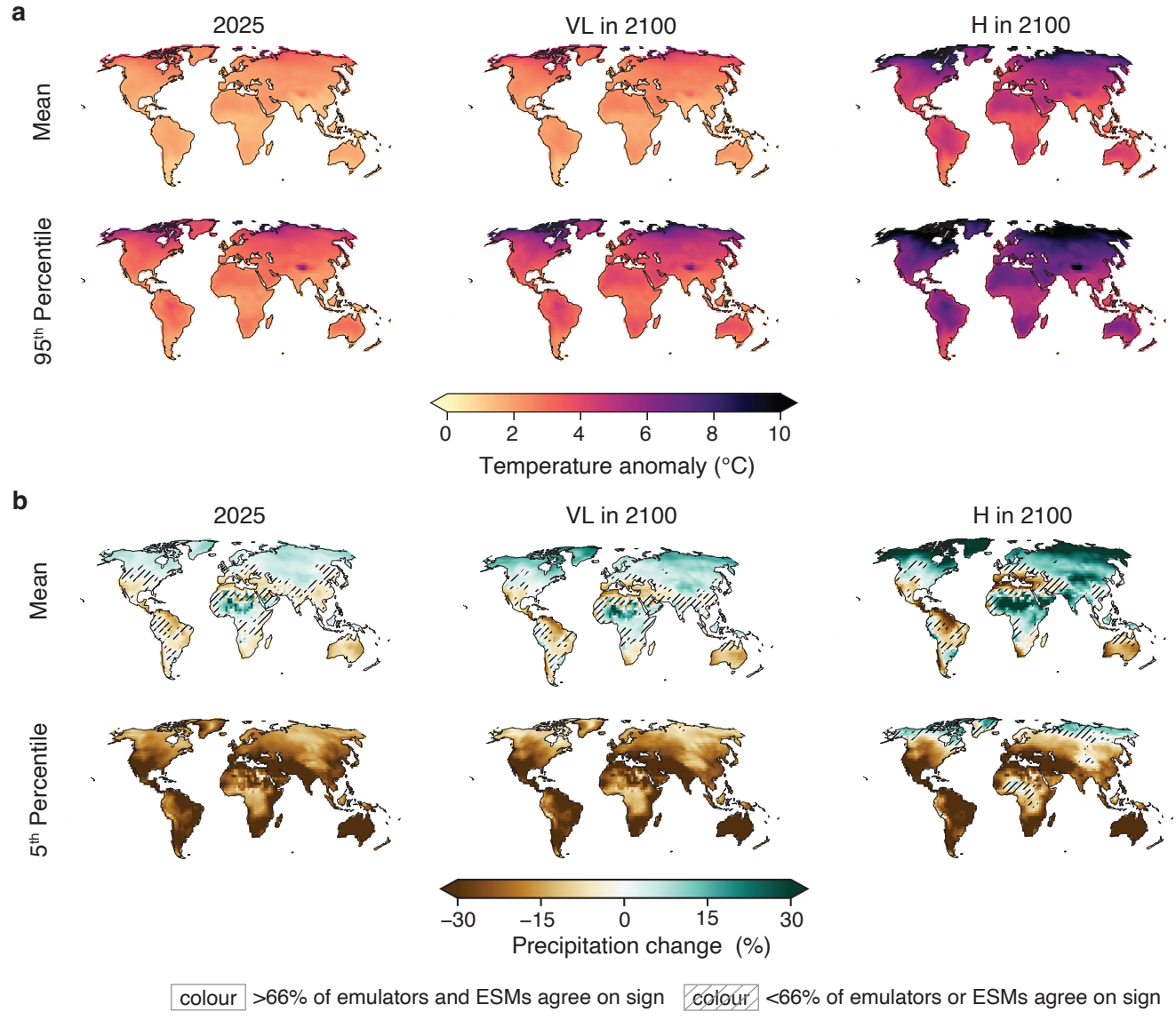


Figure 3. Spatial distribution of emulated temperature and precipitation. a, Annual mean temperature anomaly relative to pre-industrial for present day (2025, left) and for VL (middle) and H (right) in 2100, from the multi-emulator ensemble. Top: ensemble mean. Bottom: 95th percentile, i.e. the temperature exceeded in the hottest 5 % of realisations. **b**, Same as **a**, but for annual precipitation change, showing the ensemble mean (top) and the 5th percentile (bottom), i.e. the value undercut in the driest 5 % of realisations. Hatching indicates regions where fewer than 66 % of ESMs and emulators agree on the sign of change.

https://doi.org/10.5194/egusphere-2026-6328
Preprint. Discussion started: 16 November 2026
© Author(s) 2026. CC BY 4.0 License.

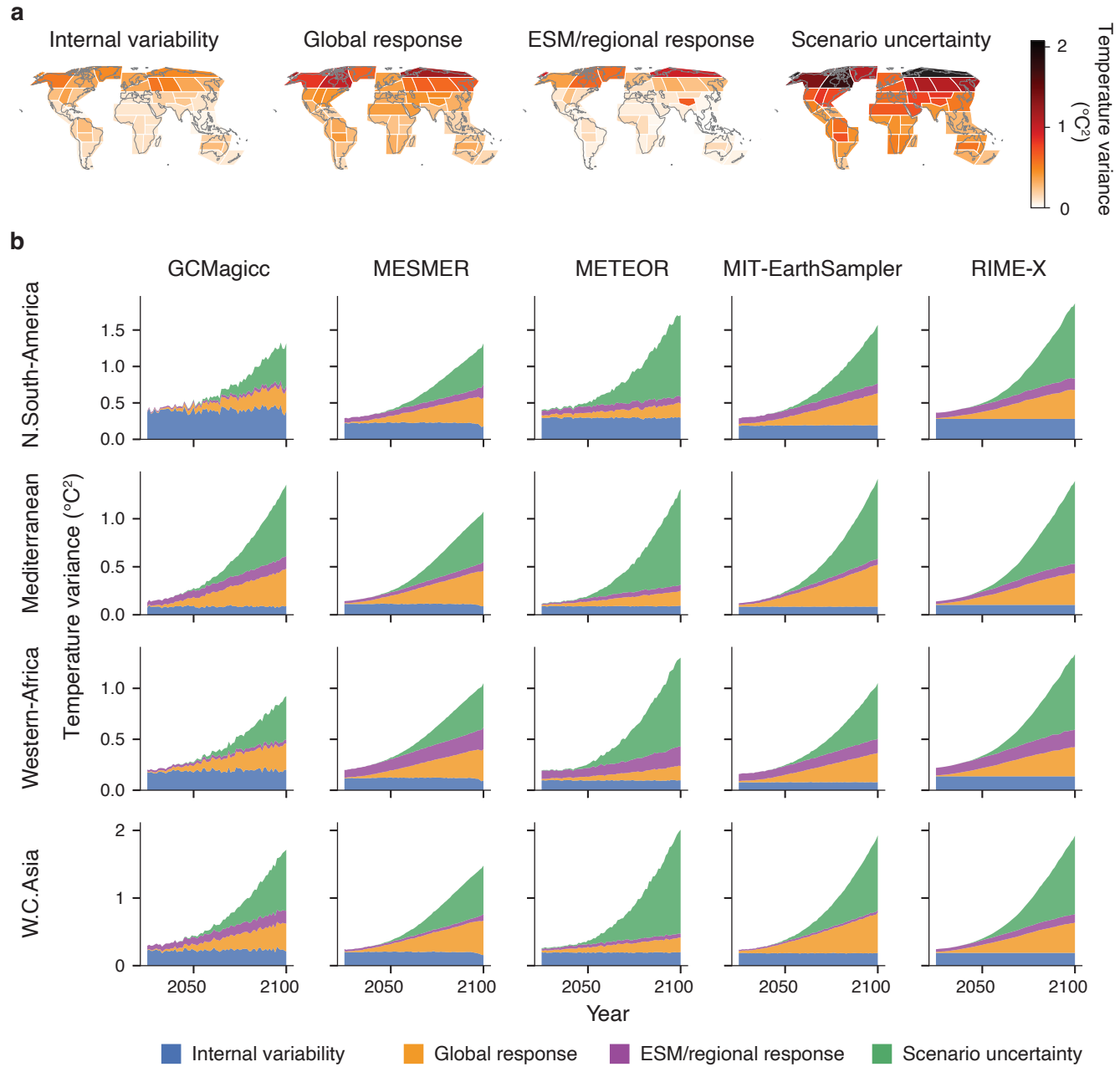


Figure 4. Decomposition of uncertainty in emulated annual temperature. a, Variance of regional annual mean temperature in 2100 attributed to internal variability, global response, ESM/regional response and scenario uncertainty, estimated for each emulator with a nested analysis of variance (ANOVA) and averaged across emulators. Regions follow the IPCC AR6 reference regions (Iturbide et al.). Global response denotes uncertainty in the global temperature response to a given emission pathway as estimates by FaIR (Smith, 2026); ESM/regional response denotes differences in the regional pattern across ESMs. **b**, Evolution of the same variance components from 2025 to 2100 for four example regions (rows) and each emulator (columns).

https://doi.org/10.5194/egusphere-2026-6328
Preprint. Discussion started: 16 November 2026
© Author(s) 2026. CC BY 4.0 License.

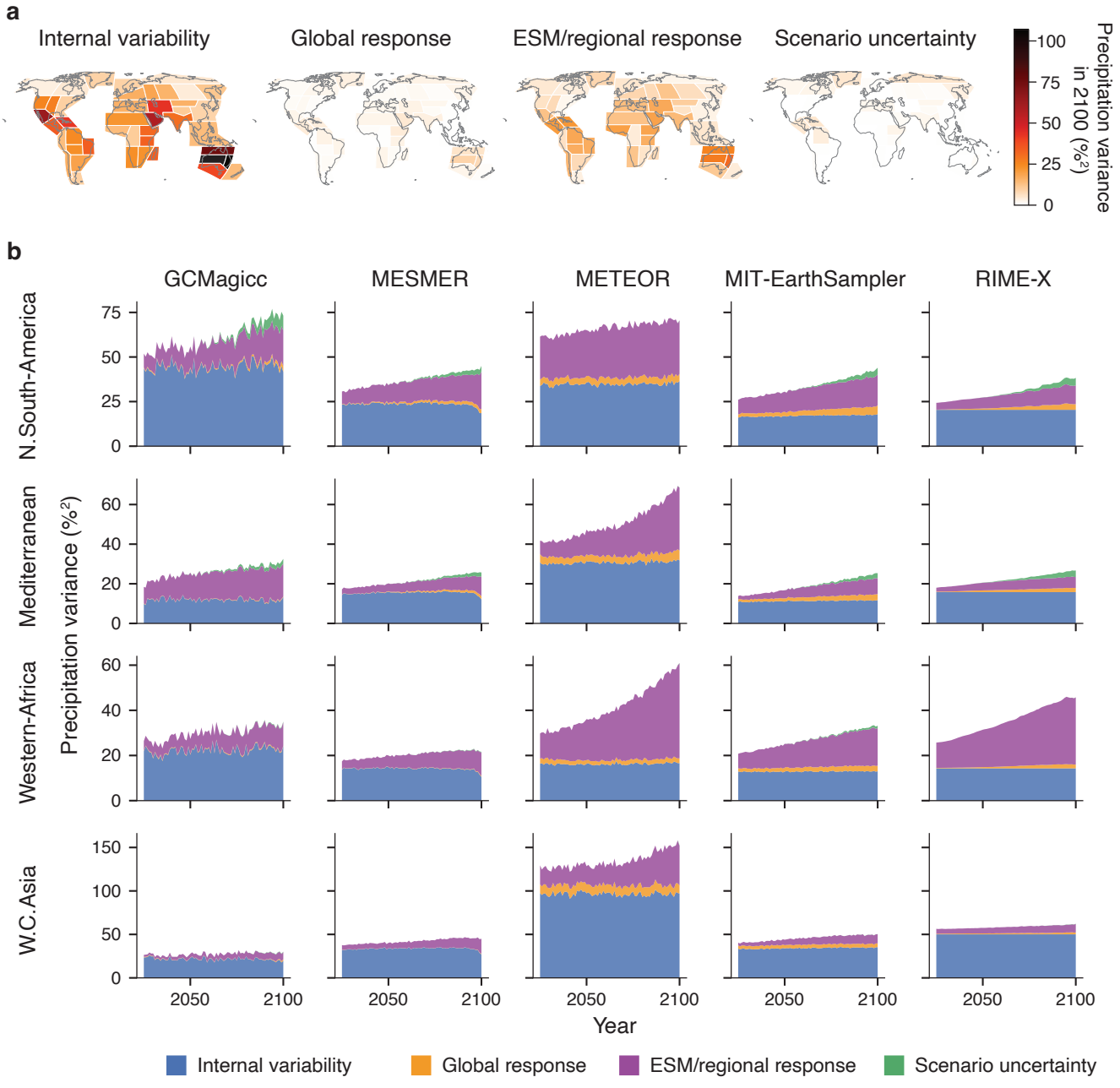


Figure 5. Decomposition of uncertainty in emulated annual precipitation. Same as Fig. 4, but for annual precipitation change (variance in $\%^2$).

https://doi.org/10.5194/egusphere-2026-6328
Preprint. Discussion started: 16 November 2026
© Author(s) 2026. CC BY 4.0 License.

regional translation, such revisions can be propagated to regional projections by re-running the emulators with a recalibrated SCM version, within days and without new ESM simulations. Note, the representation of global climate uncertainty can vary from emulator to emulator depending on the chosen sampling strategy. For example, METEOR works with a subsample of 20 FaIR configurations, GCMAgicc, MESMER, and MIT-EarthSampler all work with 100, and PRIME relies on all 841. These choices in sampling strategies translate into varying contributions of global response uncertainty to overall uncertainties.

For precipitation, the decomposition of uncertainties is almost reversed. Internal variability and the ESM-specific regional response dominate across regions and emulators, the global response is small, and scenario uncertainty is about an order of magnitude smaller still (Fig. 5). The MIT-EarthSampler again shows the smallest contribution of internal variability, and METEOR and GCMagicc the largest, depending on region. This is consistent with the well-documented difficulty of constraining regional precipitation responses (Hawkins and Sutton; Shepherd, 2014). Because the decomposition was performed on log-transformed precipitation, the reported shares are relative shares in log space and may overstate internal variability in dry regions (Methods).

4.2 Scenario differences

Despite these uncertainties, the scenarios lead to clearly different regional climates (Figs. 3 & 6). Land warms faster than the ocean (Sutton et al., 2007): global land temperature reaches 2.3 °C (1.4–3.4 °C) under VL and 3.9 °C (2.8–5.3 °C) under M in 2100, about 1.4 times the global mean. Polar amplification (Serreze and Barry, 2011) further increases warming at high northern latitudes. Under M, warming reaches 5.7 °C (3.3–8.1 °C) in North-Western and 6.3 °C (3.8–9.0 °C) in North-Eastern North America, and the 95th percentile under H exceeds 8 °C over much of the Arctic land (Fig. 3a). Warming also exhibits seasonal variations, with the strongest warming at northern latitudes during boreal winter (December–February; Fig. 8a). Throughout regions, warming under VL and L remains substantially below that under M and H (Fig. 6). The global land-mean temperature of even the coolest 5% of years under M is above the hottest 95% of years observed today.

Precipitation changes are more heterogeneous and less robust (Fig. 3). Parts of the tropics, particularly regions in Western- and Central-Africa, and the high latitudes experience a robust wetting as warming accelerates, whereas the Amazon, the Mediterranean, parts of Southern North America and western Australia experience robust drying (Fig. 3b). The wetting signals over India are only robust under very high warming (e.g., under H in 2100), while results over Eastern Asia are robust under low warming with models disagreeing over the sign under strong warming trends. Under M in 2100, The strongest relative wetting occurs at high northern latitudes, for example 26 % (9–50 %) in the Greenland–Iceland region. Drying is largest in Northern South America, Southern Central America and the Mediterranean, with changes of -16 % (-35 to $+5$ %), -16 % (-38 to $+7$ %) and -15 % (-30 to $+4$ %) relative to pre-industrial (Fig. 7). Under VL, these reduce to -10 % (-30 to $+8$ %), -9 % (-29 to $+12$ %) and -10 % (-23 to $+6$ %). In each of these three regions, models project that we have reached a mean precipitation decline between -7 to -8 % already today, meaning the additional drying under M relative to present-day is more than 2.5 times and up to almost 4 times that of the drying under VL. These drying trends persist across seasons, but vary by magnitude with the strongest drying in northern South America from September through November, while the drying over southern Central America is most pronounced from June through August (Fig. 8b). Within these drying regions lie part of the

https://doi.org/10.5194/egusphere-2026-6328
Preprint. Discussion started: 16 November 2026
© Author(s) 2026. CC BY 4.0 License.

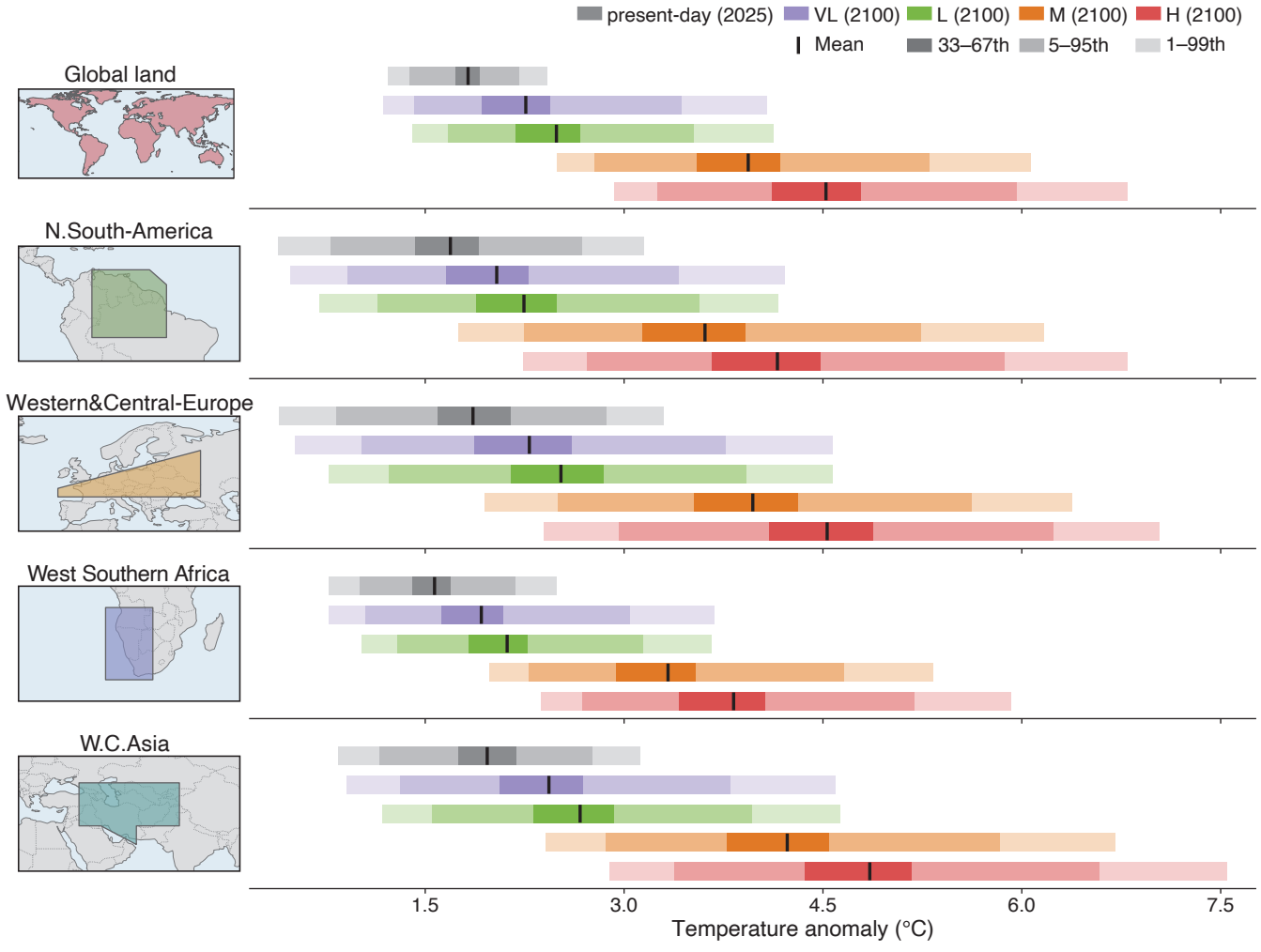


Figure 6. Regional distributions of emulated temperature. Distributions of annual mean temperature anomaly relative to pre-industrial over global land and four example regions for present day (2025, grey) and for VL (purple), L (green), M (orange) and H (red) in 2100. Bars show the 33rd–67th (dark), 5th–95th (medium) and 1st–99th (light) percentile ranges, and black ticks the mean, pooled across emulators, ESMs and realisations.

https://doi.org/10.5194/egusphere-2026-6328
Preprint. Discussion started: 16 November 2026
© Author(s) 2026. CC BY 4.0 License.

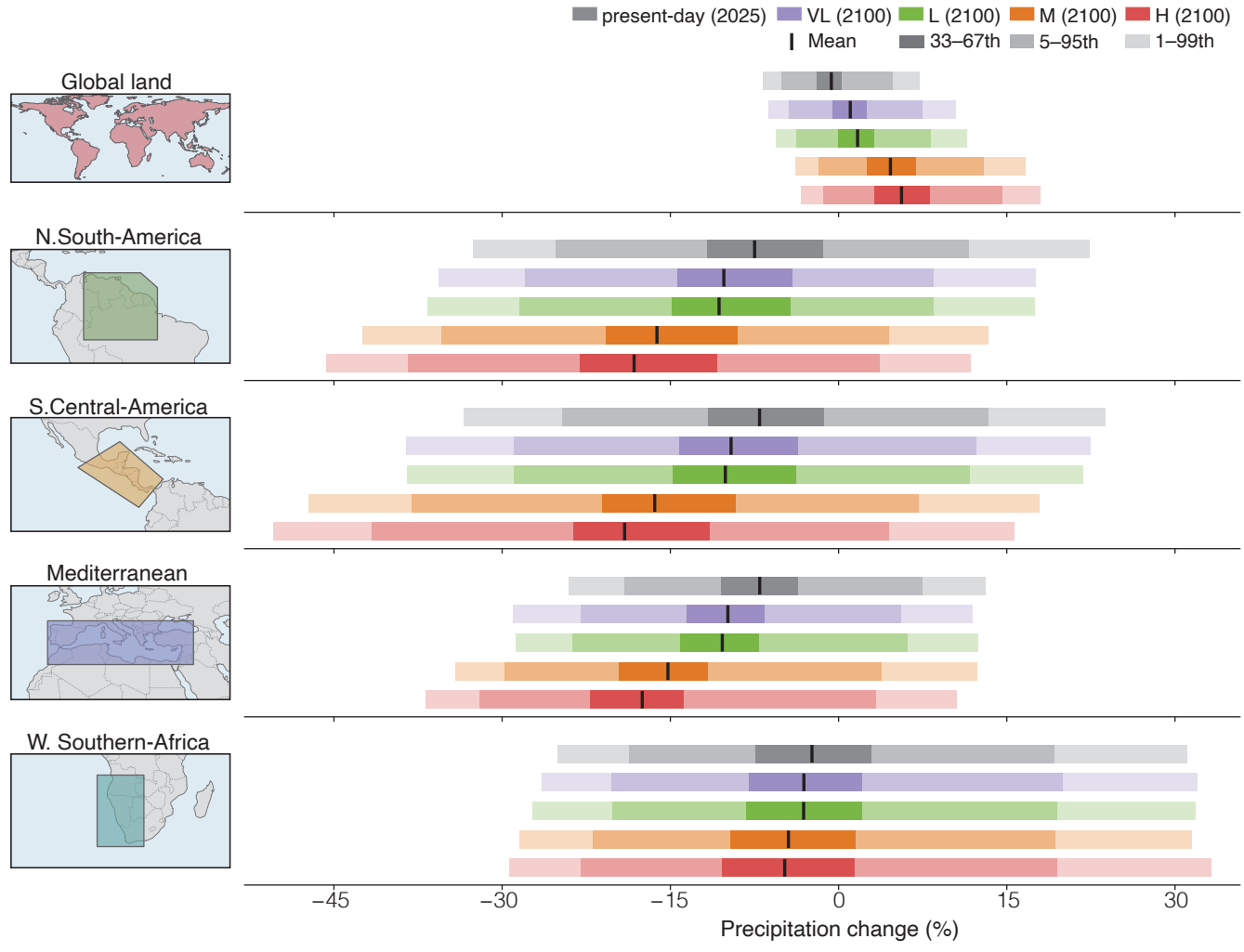


Figure 7. Regional distributions of emulated precipitation. Same as Fig. 6, but for annual precipitation change (%) and a different set of example regions.

https://doi.org/10.5194/egusphere-2026-6328
Preprint. Discussion started: 16 November 2026
© Author(s) 2026. CC BY 4.0 License.

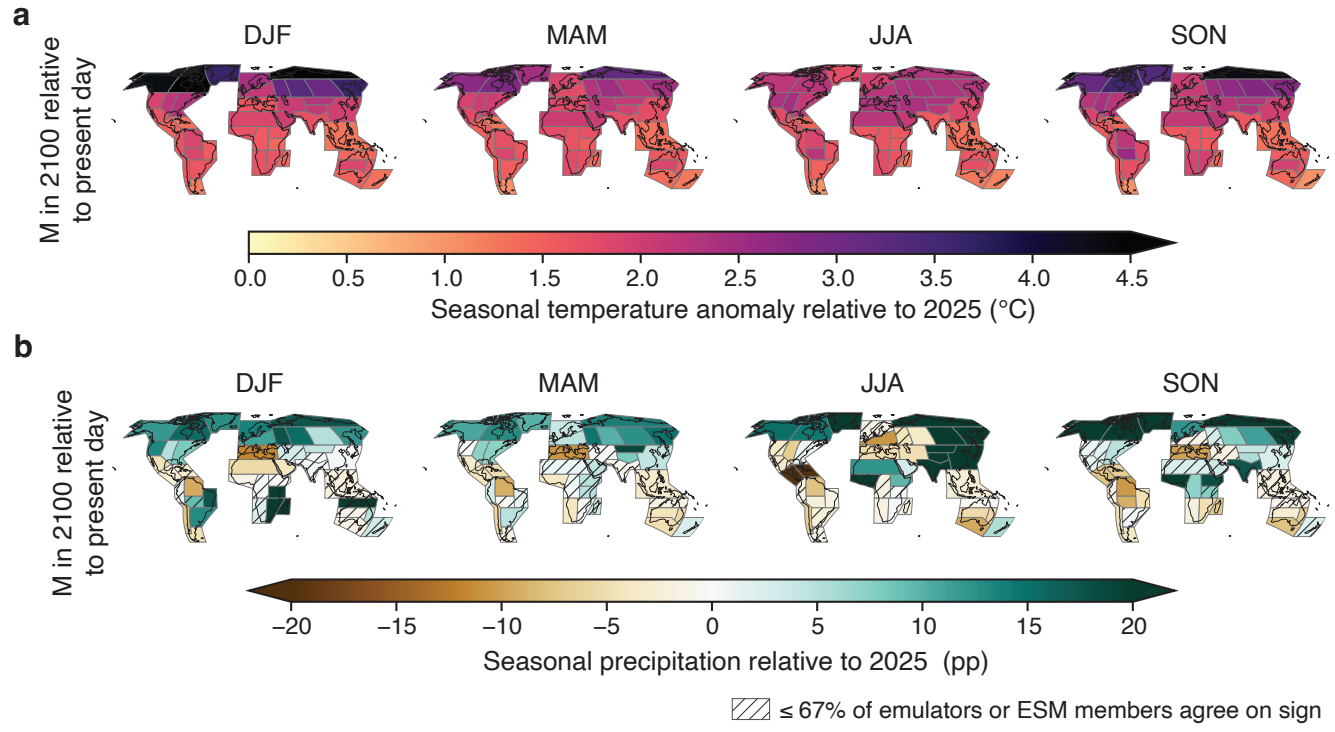


Figure 8. Seasonal variation of temperature and precipitation changes under M in 2100 relative to present-day. a, Temperature change under M in 2100 relative to present-day (2025). **b**, Same as **a** but for precipitation. The deviations then represent changes in percentage points by season with the overall percentage scores being relative to the 1850-1900 annual climatology.

Amazon rainforest, which suffered two consecutive, record-breaking droughts in 2023–2024 (Bai et al., 2026), and already experiences potential early-warning signals of rainforest dieback (Bochow and Boers, 2023).

5 Diagnosing differences between emulators

When emulators are used to extend ESM ensembles to new scenarios, each emulator's structural assumptions and training choices add a further layer of uncertainty. Here we quantify how large this layer is relative to ESM uncertainty, and what drives it.

5.1 Emulator uncertainty relative to ESM uncertainty

We decompose the variance in median emulated estimates, by AR6 land region and scenario, into contributions from ESM choice, emulator choice, and their interaction using an ANOVA decomposition (see Methods). We apply it to three 25-year periods (2025–2050, 2050–2075 and 2075–2100); averaging over these periods reduces the influence of interannual variability.

https://doi.org/10.5194/egusphere-2026-6328
Preprint. Discussion started: 16 November 2026
© Author(s) 2026. CC BY 4.0 License.

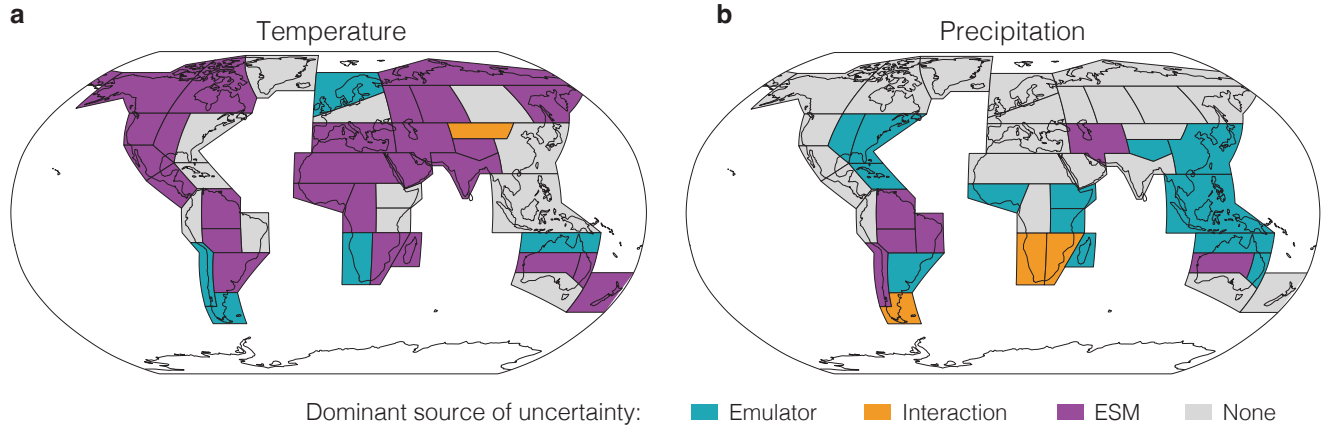


Figure 9. Relative importance of ESM versus emulator choice in the variance decomposition. Colours indicate the dominant source of variance among ESM choice, emulator choice, and their interaction. Regions with a consistent dominant source across all scenarios (VL, L, M, H) and time periods (2025–2050, 2050–2075, 2075–2100) are shown by the corresponding colour, while grey indicates regions in which the dominant source varies across scenarios and/or time periods. **(a)** Temperature and **(b)** precipitation.

For temperature, ESM choice is the dominant source of variance in most regions (Fig. 9a). Across all scenarios and periods, 26 regions are consistently dominated by ESM choice, 5 by emulator choice and 1 by ESM–emulator interaction. The remaining regions switch between dominant sources depending on scenario and period. For example, Southeast Asia shifts from ESM-dominated variance early in the century to emulator-dominated variance from mid-century onwards, while North Eastern Africa is interaction-dominated at low warming and ESM-dominated at high warming. The regional partitioning is most similar within the M–H and L–VL scenario pairs (Fig. S2 in the Supplement).

For precipitation (log-ratio change relative to 1850–1900; PRIME excluded owing to faulty data), the balance is reversed (Fig. 9b). Emulator choice dominates in 13 regions across all scenarios and periods, compared with 6 regions dominated by ESM choice and 3 by interaction. The margin between the largest and second-largest source is greatest under high-warming scenarios towards the end of the century, in Eastern Australia and parts of the tropics such as Southeast Asia and Eastern Africa (Fig. S1 in the Supplement). Thus, while regional temperature uncertainty is shaped mainly by differences between ESMs, for precipitation the choice of emulator matters more than the choice of ESM in many regions.

5.2 Emulator disagreement

To locate where emulator-induced uncertainty arises, we compare local-to-global warming relationships across ESMs and emulators (Fig. 10). If an emulator reproduced its training ESMs perfectly, its inter-ESM spread (Fig. 10a) would roughly match that of the underlying CMIP6 simulations. However, neither model reproduces this pattern. GCMagicc, MESMER and PRIME understate the inter-ESM spread, most visibly over tropical South America, where the CMIP6 ESMs disagree most.

https://doi.org/10.5194/egusphere-2026-6328
Preprint. Discussion started: 16 November 2026
© Author(s) 2026. CC BY 4.0 License.

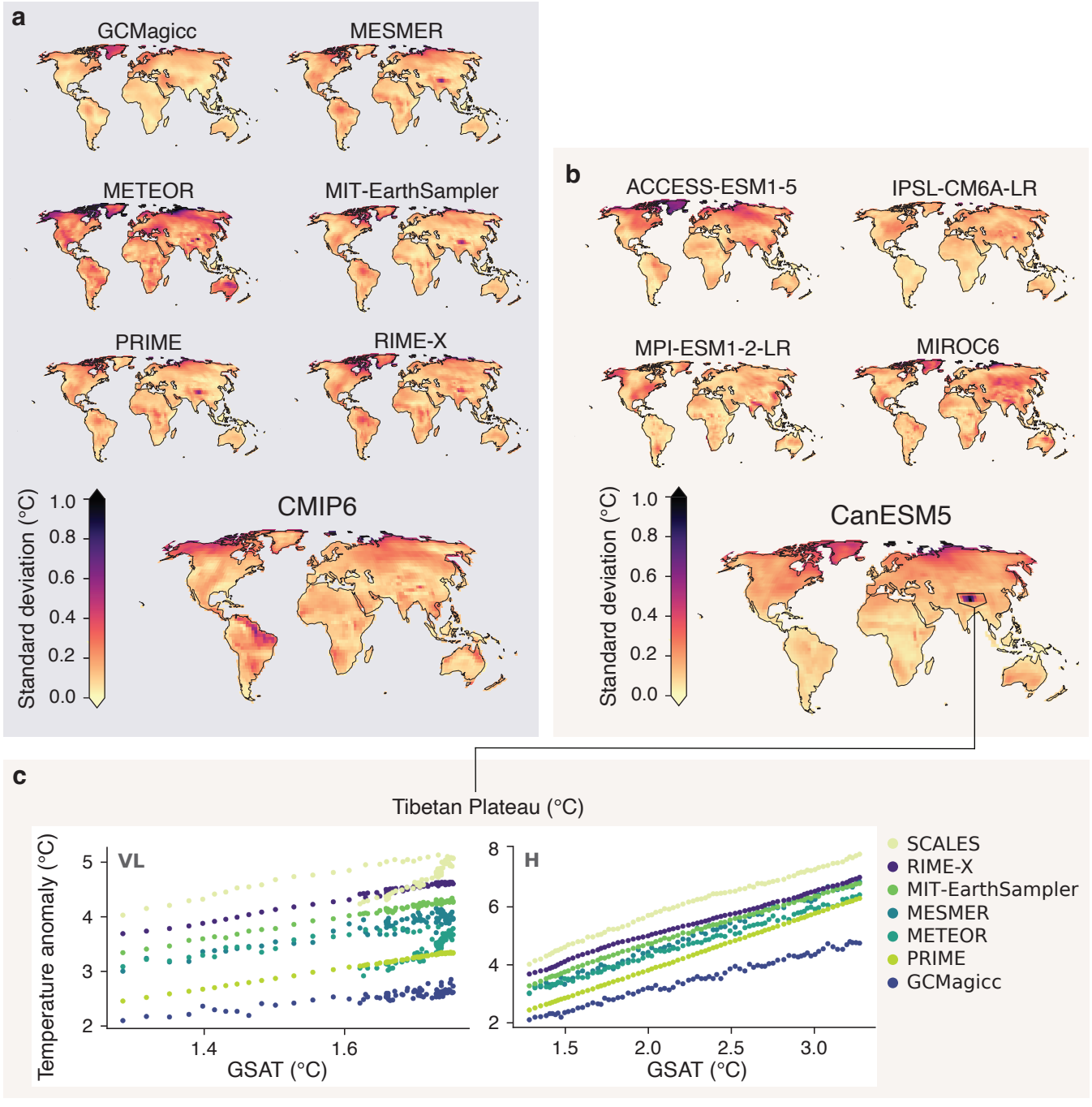


Figure 10. Spread in local-to-global warming relationships across ESMs and across emulators. a, For each emulator, the standard deviation across Tier 1 ESMs of the local-to-global warming relationship. This relationship is the linear response coefficient of local warming to GSAT, computed for each emulator, ESM and scenario and then averaged across scenarios. The CMIP6 panel shows the same quantity computed from the original Tier 1 ESM simulations. **b**, As in **a**, but for each ESM, the standard deviation across emulators. **c**, Regional versus global warming over the Tibetan Plateau (outlined in the CanESM5 map in **b**) for emulations of CanESM5 under the VL (left) and H (right) scenarios. Each point shows, for one emulator and one time step, the scenario-mean regional warming plotted against the scenario-mean GSAT.

https://doi.org/10.5194/egusphere-2026-6328
Preprint. Discussion started: 16 November 2026
© Author(s) 2026. CC BY 4.0 License.

METEOR overstates it over the Arctic, northern Eurasia and Australia. Several emulators (MESMER, MIT-EarthSampler, PRIME and RIME-X) also show a pronounced spread maximum over the Tibetan Plateau that is absent from the CMIP6 data.

Taking the spread across emulators for each ESM instead (Fig. 10b) shows that the size of the emulator uncertainty depends on the ESM being emulated. Emulators agree closely for IPSL-CM6A-LR but diverge more for ACCESS-ESM1-5 (Greenland and the North Atlantic), MIROC6 (Eurasia) and MPI-ESM1-2-LR (North-Eastern North America). For CanESM5, inter-emulator spread over the Tibetan Plateau reaches the top of the colour scale, meaning the Tibetan hotspot in Fig. 10a arises mainly because the emulators disagree about the regional warming signal in a single ESM, namely CanESM5.

5.3 Structural and training contributions to emulator disagreement

For the Tibetan Plateau under CanESM5 (Fig. 10c) and H, all emulators produce near-linear regional-to-global relationships, but these are offset from one another by 2–3 °C at the same GSAT, with GCMagicc and SCALES at the lower and upper ends. Although GCMagicc's relationship is markedly shallower, most of the disagreement comes from the offset rather than the slope coefficients. Under VL, where GSAT peaks and declines, the emulators also differ in the shape of the response. SCALES and METEOR show hysteresis, with regional warming declining faster after the GSAT peak than it increased before it. MESMER and GCMagicc produce scatter around their mean relationship, which represents effects of natural variability for MESMER (pattern-scaling based emulator), while it could represent features of the long-term response in GCMagicc (ML-based emulator). RIME-X, MIT-EarthSampler and PRIME remain close to linear.

The differences in warming responses under VL, a mild peak-and-decline scenario with overshoot, are partially driven by structurally different assumptions. METEOR, for instance, separates the response into greenhouse-gas and aerosol impulse-response patterns, which often produces hysteresis at the regional scale. This can add value where local hysteresis is present in the parent ESM (e.g., West & Central Europe in MIROC6), but it can also exceed, or appear without, the corresponding signal in the source ESMs (e.g., North-West North America under ACCESS-ESM1-5). ML-based emulators such as SCALES and GCMagicc impose no fixed response shape and can therefore capture a range of behaviours: both project linear relationships in some regions (e.g., the Mediterranean for ACCESS-ESM1-5) and hysteresis in others (e.g., Greenland and Iceland for CanESM5). The conditional resampling in RIME-X can also lead to hysteresis signals if those are present within the training distribution.

Structure explains only part of the spread, however; the data used for training, testing and validation also shape emulator output. MESMER, MIT-EarthSampler and PRIME share a linear pattern-scaling prior for the forced response, so the differences between them in Fig. 10c arise mainly from training choices, such as which ensemble members and scenarios are used. Over the Tibetan Plateau these differences appear mostly as an offset, but training choices can equally change the regional-to-global scaling itself: in the Caribbean under CanESM5, MESMER estimates a slope of 0.61 and MIT-EarthSampler 0.85, compared with 0.84 in the CMIP6 data. Such comparisons are not like-for-like, because training set-ups differ widely. We return to this point in the Discussion.

https://doi.org/10.5194/egusphere-2026-6328
Preprint. Discussion started: 16 November 2026
© Author(s) 2026. CC BY 4.0 License.

6 Methods

The FASTMIP-CMIP7 experiment follows a shared protocol design described in Section 2. Instead of requesting the full output, each group processes their data independently to produce a set of common outputs. For each scenario, variable, and tier, participating groups provide gridded output ($2.5° \times 2.5°$ resolution; 1850–2023 for the historical period and 2024–2100 for projections) as two sets of quantiles (mean, median, and the 1st, 2.5th, 5th, 33rd, 67th, 95th, 97.5th, and 99th percentiles): one describing spread within each individual ESM-calibrated emulator, and one describing spread across the multi-model ensemble. In addition, groups provide a decomposition of total uncertainty into scenario, global and regional response, and internal variability components (and, where applicable, socioeconomic uncertainty), following the decomposition framework of (Hawkins and Sutton). All outputs are archived with metadata documenting the FaIR configuration used to force each emulator, enabling reproducibility across the multi-emulator ensemble. Here, we first describe the decomposition of uncertainties (Section 6.1) and then describe the modelling workflows from each of the participating emulators (Section 6.2).

6.1 Uncertainty decomposition

We decompose the spread of the emulated ensembles into contributions from internal variability, the regional ESM response, the global climate response and scenario choice, following Hawkins and Sutton. Let $X_{s,m,f}(t)$ denote the emulated annual value of a variable in year t for scenario s, ESM m and FaIR ensemble member f, either at grid-cell level or as an area-weighted (cosine-latitude) mean over an AR6 land region.

Each realisation is separated into a forced response $F_{s,m,f}(t)$ and a residual $R_{s,m,f}(t) = X_{s,m,f}(t) - F_{s,m,f}(t)$, which represents internal variability. Where an emulator provides several internal-variability realisations per forced trajectory, F is estimated as the mean across these realisations and the internal variability as the variance across them. MESMER provides a single variability realisation per FaIR member, so we instead estimate F by fitting a fourth-order polynomial in time to each series over 2024–2100, as in Hawkins and Sutton. The four variance components are then

$$V_{\mathrm{int}}(t) = \overline{\mathrm{Var}_f\left[R_{s,m,f}(t)\right]}^{m}, \tag{1}$$

$$V_{\mathrm{ESM}}(t) = \overline{\mathrm{Var}_m\left[F_{s,m,f}(t)\right]}^{f}, \tag{2}$$

$$V_{\mathrm{glob}}(t) = \mathrm{Var}_f\left[\overline{F_{s,m,f}(t)}^{m}\right], \tag{3}$$

$$V_{\mathrm{scen}}(t) = \mathrm{Var}_s\left[\overline{F_{s,m,f}(t)}^{m,f}\right], \tag{4}$$

where overbars denote means over the indicated dimensions and V_{int}, V_{ESM} and V_{glob} are computed for each scenario and averaged across scenarios. Internal variability V_{int} is the variance of the residuals across realisations, averaged over ESMs. The ESM (regional response) term V_{ESM} is the variance of the forced response across ESMs for a given FaIR member, averaged over members. The global-response term V_{glob} is the variance across FaIR members of the multi-ESM mean forced response. Together, V_{ESM} and V_{glob} add up exactly to the total variance of the forced response across ESMs and FaIR members (law of total variance), with any ESM–FaIR interaction attributed to the ESM term. Scenario uncertainty V_{scen} is the variance across scenarios of the mean forced response. The ESM term is computed for the five Tier 1 ESMs, and separately for all Tier 1 and

https://doi.org/10.5194/egusphere-2026-6328
Preprint. Discussion started: 16 November 2026
© Author(s) 2026. CC BY 4.0 License.

Tier 2 ESMs where available. For precipitation, all components refer to variance in log space, so they cannot be converted directly into variances of absolute changes.

6.2 Participating Spatially Explicit Emulators

6.2.1 GCMagicc

GCMagicc (Meinshausen et al., 2026a) is a spatially explicit climate emulator that pairs a SCM with a machine-learning generative model to produce spatially-resolved, multivariate climate output at Earth-System-Model-like resolution [add citation when preprint is out]. We here rely on the GCMagicc-PM configuration which is retrained independently on each CMIP6 model's historical run and uses a reduced predictor set of decomposed effective radiative forcing (ERF) components, model index and seasonal descriptors. The model jointly generates ten monthly variables (tas, pr, tasmax, tasmin, hurs, huss, psl, rsds, sfcWind, ts) on a hierarchical HEALPix grid, combining deterministic bias terms with a stochastic generator trained via an energy-score objective, producing spatio-temporally coherent (cross-variable) realizations. The generated data is then regreidded to the 2.5°x2.5° equal latitude-longitude grid.

In place of MAGICC, we force GCMagicc-PM with data from FaIR and we do not use GCMagicc's ERA5-splicing or observational-alignment features. All data were generated with GCMagicc v1 (Meinshausen et al., 2026b), available via Github at https://github.com/maltemeinshausen/GCMagicc_v1_manuscript under the Apache License 2.0 (Meinshausen et al., 2026a).

6.2.2 MESMER

The Modular Earth System Model Emulator with spatially Resolved output (MESMER) is a spatially-resolved climate emulator that translates annual mean climate trajectories into gridded fields of selected climate variables over land (Beusch et al., 2020b; Nath et al., 2022; Quilcaille et al., 2023; Schöngart et al., 2024). It is an ESM-specific emulator and, depending on the availability of ESM data for a specific variable, trained on 26-72 CMIP6 models. The modelling framework accounts for the local forced climate response as well as internal variability of the respective ESM and produces spatio-temporally coherent (cross-variable) realizations. Individual MESMER modules have been combined into a versioned software package, available on Github: https://github.com/MESMER-group/mesmer/releases/tag/v1.0.0 (Bauer et al., 2026).

MESMER modules include: (i) annual mean land surface air temperature (core), (ii) extension to monthly gridded mean temperatures (MESMER-M), (iii) extension to monthly precipitation, coherent with temperature (MESMER-M-TP), (iv) climate extremes and climate impact drivers, for example, annual maximum temperature, soil moisture or fire weather index (MESMER-X).

MESMER was forced with a subset of 100 FaIR trajectories selected using an uncertainty preserving clustering algorithm specifically developed for coupling MESMER to SCMs (Schwaab et al., 2024). MESMER is trained to work with forced climatic responses and adds ESM-specific global variability to these forced responses internally (Beusch et al., 2020b). All data was generated with MESMERv1.0.0 (Bauer et al., 2026), available via Github or (Hauser et al., 2026) along with its

https://doi.org/10.5194/egusphere-2026-6328
Preprint. Discussion started: 16 November 2026
© Author(s) 2026. CC BY 4.0 License.

pre-trained parameters (Quilcaille et al., 2026). These parameters were computed by training on a single ensemble member across scenarios.

6.2.3 METEOR

METEOR (Multivariate Emulation of Time-Evolving and Overlapping Responses) is a spatially resolved emulator which natively takes global emissions and concentrations fields, computes corresponding forcing trajectories and translates them into gridded ESM-emulating fields (temperature and precipitation so far) using an impulse response assumption with multiple timevolving separate GHG and aerosol forcing induced pattern responses (Sandstad et al., 2025). The updated version used here (Sanderson et al., 2026b) adds onto that grid-resolved seasonal responses and VAR-X PCA-based patterns to enable production of monthly outputs with ensemble variability trained from the ESM. This version includes the option calculate impacts variables such as heating degree and cooling degree days, and has the option of taking in a GSAT timeseries for scaling of results to fit a global mean temperature trajectory.

METEOR is openly available from Github: https://github.com/benmsanderson/METEOR.git and we used version v1.6.1.

Training of METEOR is performed per model using monthly ESM output from a single ensemble member for the experiments piControl, abrupt-4xCO2, historical and ssp245 (a different scenario could also be used).

6.2.4 MIT-EarthSampler

MIT-EarthSampler is a spatially-resolved climate emulator that translates annually and globally averaged temperature trajectories into gridded fields of selected climate variables (Bouabid et al., 2026). It is an ESM-specific emulator trained on 5 CMIP6 models, producing realizations of monthly climate fields for near-surface air temperature, precipitation, relative humidity, and wind speed. The modelling framework accounts for the local forced climate response as well as internal variability of the respective ESM and accurately captures both cross-variable correlations at the grid-cell level and spatial correlations within each variable. MIT-EarthSampler is available as a software package on Github, and all data was produced with MIT-EarthSamplerv0.1.12: https://github.com/shahineb/mit-earthsampler.

6.2.5 PRIME

The Probabilistic Regional Impacts from Model patterns and Emissions (referred to as PRIME) (Mathison et al., 2025) is a spatially-resolved climate emulator that is designed to reproduce the spread and distribution that would be output from CMIP6 for the scenarios, but without the need for long ESM runs or all the inputs that are needed for these more complex models. PRIME uses the emissions that are typically used as inputs to SCMs and run FaIR as part of the PRIME framework to provide a distribution of temperatures. PRIME then provides the capability to include features of the most recent ESM projections, science, and scenarios to run ensemble simulations on multi-centennial timescales and include analysis of many key variables that are relevant and important for impacts assessments. These estimated temperatures are used to scale monthly-mean patterns from a large number of CMIP6 ESMs, selected to suit the users need. These patterns then provide the inputs to a "weather

https://doi.org/10.5194/egusphere-2026-6328
Preprint. Discussion started: 16 November 2026
© Author(s) 2026. CC BY 4.0 License.

generator" algorithm and a land-surface model JULES. The PRIME system thus generates an end-to-end estimate of the land-surface impacts from the emissions scenarios. The PRIME system can be run in a similar way to an ESM using Rose, (J Oliver et al., 2018; Shin et al., 2024) – a group of utilities and specifications which provide a common way to manage the development and running of scientific application suites in both research and production environments.

6.2.6 RIME(-X)

RIME (Byers et al., 2025) is a climate impact emulator designed for rapid scenario assessment including for the integrated assessment modeling community that translates GSAT timeseries from SCMs into timeseries of regionally aggregated climate impacts, using a database of regional climate impact drivers and sectoral impacts at discrete GSAT levels and linear interpolation between them. RIME-X (Schwind et al., 2026a) is its probabilistic extension, translating probabilistic GSAT ensembles from SCMs directly into probabilistic regional climate impact information that jointly quantifies global climate response uncertainty, the uncertainty in translating global climate conditions into regional indicators, and natural variability. It combines scenario- and time-dependent GSAT distributions, used as priors, with region-dependent indicator distributions conditional on GSAT retrieved from an ensemble of Earth system model simulations, used as conditionals, to derive scenario-, time-, and region-dependent marginal distributions that quantify the full uncertainty space of how a given regional climate or climate impact indicator could evolve under climate change. RIME-X is conceptually applicable to regional indicators whose distributions are predominantly determined by a global warming level. The version in this paper is the one archived on Zenodo (Schwind et al., 2026b), calibrated on all available historical simulations as well as the SSP126, SSP245, SSP370, SSP460, and SSP585 scenario simulations across the CMIP6 next-generation archive (Brunner et al., 2020) for the given set of ESMs using equal model weighting. RIME-X is available as an open-source package that is continuously updated and includes a tutorial, available at https://github.com/iiasa/rimeX.

6.2.7 SCALES-MESH

SCALES-MESH (Kain et al., 2026) is an AI-based, modular and hierarchical climate emulator framework that combines regional projections with downscaling. Its SCALES module translates projections of GSAT into regional monthly temperature and precipitation anomaly projections aggregated over the IPCC-AR6 regions, while its MESH module performs spatial downscaling of those projections to gridded fields at 2.5° resolution. SCALES is based on a state space model that transforms the GSAT trajectory into a trajectory of latent states, which condition a diffusion transformer that generates a timeseries of monthly regional temperature and precipitation anomaly vectors at the AR6 region scale through diffusion with partial infilling, similar to how panorama images are generated. SCALES captures distributional properties, including distribution shapes and spatial, inter-variable, and temporal correlations, as well as trends, including path-dependency effects. MESH is a conditional diffusion model based on a vision transformer that downscales the monthly precipitation and temperature fields generated by SCALES to a 2.5° resolution grid. SCALES-MESH can further emulate across several ESMs jointly using a neural process learning approach. SCALES-MESH will be made available open source (repository forthcoming); the version used here is trained on all available simulations for the historical, 1pctCO2 and abrupt4xCO2 experiments as well as the SSP119, SSP126,

https://doi.org/10.5194/egusphere-2026-6328
Preprint. Discussion started: 16 November 2026
© Author(s) 2026. CC BY 4.0 License.

SSP245, SSP370, SSP460, SSP534-over and SSP585 scenarios for the primary ESMs of FastMIP available in the CMIP6 next-generation archive (Brunner et al., 2020), as well as 40 SSP126 and SSP534-over simulations extended until 2300 (Ziehn et al., 2019), flat10MIP (Sanderson et al., 2026a) and ZECMIP (Jones et al., 2019) data for the ACCESS-ESM1-5 model.

7 Discussion

FASTMIP-CMIP7 demonstrates how climate emulators can extend the scope of scenario-based climate projections by generating large ensembles across emissions pathways and ESMs at a fraction of the computational cost of ESM simulations. Our results highlight three main findings. First, the limited and uneven ensemble sizes available from CMIP6 ESMs can lead to substantial sampling errors in regional distributions, particularly in their tails, whereas emulators make much larger samples computationally feasible. Second, the relative importance of different sources of projected uncertainty differ between variable and time horizon with scenario uncertainty playing the largest role for temperature towards the end-of-century of the century (Lehner et al.). Third, the uncertainty introduced by emulator choice is not negligible and varies by variable and region, reflecting differences in both model structure and training data.

7.1 Applications of emulated data

The capabilities of emulators open opportunities for scenario exploration, attribution, risk assessment and impact modelling: large emulated ensembles can characterise regional climate distributions, examine counterfactual pathways and estimate the likelihood of rare events that are difficult to sample with existing ESM simulations. Because emulators separate the global response from its regional translation, they can also propagate revised global constraints, such as recent updates to the transient climate response (Gyuleva et al., 2026; Boardman et al., 2026), to regional projections within days and without new ESM simulations, and could feed regional climate outcomes back into IAMs. Each application, however, sets its own requirements. Scenario exploration requires reliable responses to pathways absent from the training data, extreme-event analysis requires realistic tails, and impact modelling often requires higher temporal and spatial resolution than current emulators provide. The value of large emulated ensembles therefore also depends on the fidelity of the distributions they generate, particularly for extremes and for structurally novel scenarios that are poorly represented in the training data.

7.2 Sources of uncertainty and emulator choice

The dominant sources of regional uncertainty differ between temperature and precipitation. For temperature, the emission pathway dominates by the end of the century, and current policies (M) imply about five times as much additional global warming beyond today as stringent mitigation (VL). For precipitation, internal variability and ESM differences dominate, and scenario uncertainty is about an order of magnitude smaller. Mitigation nonetheless matters where signals are robust: in northern South America, southern Central America and the Mediterranean, additional drying beyond today is 2.5 to almost four times larger under M than under VL.

https://doi.org/10.5194/egusphere-2026-6328
Preprint. Discussion started: 16 November 2026
© Author(s) 2026. CC BY 4.0 License.

In both cases, emulator choice can itself be a substantial source of uncertainty. For temperature, the importance of emulator choice outweighs the choice of ESM in 5 regions, and for precipitation in 13 regions (Fig. 9). This puts weight on the choice of emulator for downstream applications, such as drought or crop yield assessments. Which emulator is suitable and what trade-off is acceptable for a given scientific question ultimately depends on the question itself.

7.3 Scenario exploration and overshoot

Reliability extrapolating to novel scenarios is of particular importance for assessments that include overshoot pathways. Under VL, GCMagicc, METEOR, RIME-X and SCALES produce differing regional responses after peak warming, with some exhibiting hysteresis while pattern-scaling-based emulators remain approximately linear by construction (Fig. 10c). Hysteresis may reflect a physical response of the parent ESM, but it can also be overstated or introduced by the emulator formulation. Peak-and-decline simulations such as SSP5-3.4-over are available for only 9 of the 25 Tier 2A ESMs, all but one with six or fewer realisations, limiting the ground truth available to evaluate emulator performance under overshoot. Given the growing relevance of overshoot pathways in policy contexts (Schleussner et al.), targeted evaluation of emulator performance under these pathways is a research priority.

Such evaluation must also account for differences in training and validation, which can affect apparent performance even among emulators with similar response formulations. MESMER is trained on a single realisation per scenario, making its comparison with CMIP6 largely out-of-sample, whereas MIT-EarthSampler, RIME-X and SCALES use all available CMIP6 simulations, making comparisons with those simulations in-sample. METEOR, trained primarily on idealised abrupt-forcing and control simulations, instead extrapolates to transient scenarios. A close match to the source ESM therefore does not, by itself, demonstrate better generalisation. These findings extend beyond FASTMIP: evaluation practices across climate emulators are largely non-comparable (Schoengart et al., 2026). The emulator community could therefore benefit from a common benchmark with a shared, pre-defined set of held-out ESM simulations and realisations that no emulator is trained on, and transparent documentation of each emulator's training data.

7.4 Large ensembles for extremes

For extremes, emulators offer large samples at negligible cost, flexibility across scenarios and the ability to resolve sampling uncertainty that ESM ensembles cannot. Their shortcomings are equally clear. Parametric emulators impose a distribution and extrapolate into the tails by assumption, whereas non-parametric emulators are constrained by the range of their training data. Even when training on a single realisation and testing against all remaining ones, at most 72 realisations per ESM and scenario are available for testing (Table S1), too few to verify the rarest events. Most emulators also operate at monthly or annual and 2.5° resolution, which misses many impact-relevant extremes, such as short-duration heat and rainfall events. Explicitly validating emulated tails, ideally against independently generated rare events such as ensemble-boosted simulations (Fischer et al., 2023), and extending emulators to higher temporal resolution are therefore priorities for extreme-event and impact applications.

https://doi.org/10.5194/egusphere-2026-6328
Preprint. Discussion started: 16 November 2026
© Author(s) 2026. CC BY 4.0 License.

7.5 Limitations and outlook

This analysis largely focuses on Tier 1 data from five ESMs and four of the seven CMIP7 scenarios, and may therefore not capture the full range of regional responses in the wider CMIP6 ensemble. Because all emulators share a common FaIR ensemble, the results inherit its calibration and do not sample differences in global response between FaIR and the individual ESMs. For precipitation, the log-ratio transform used in our decomposition treats drying and wetting asymmetrically and can inflate the apparent share of internal variability in dry regions (Methods). In addition, the uncertainty decomposition is scale dependent and should not be transferred directly to finer spatial or temporal scales (Lehner et al.).

The key priority is to pair the sampling advantages of emulators with transparent, application-specific evaluation that focuses on scenario-exploration and extremes. Coordinated benchmarking, independent testing and targeted experiments for overshoot and extremes would establish where emulated projections are robust and where uncertainty remains substantial. FASTMIP-CMIP7 provides a basis for this work by offering to run emulators under a shared protocol and allowing for a direct comparison across emulators, ESMs and scenarios. Realising the broader potential of climate emulators depends on establishing trust in emulators for the questions they are sought to answer.

Code and data availability. Most of the emulators employed in this study are open-source tools available via GitHub (see Sect. 6.2). They were calibrated on CMIP6 output publicly available via the Earth System Grid Federation (see Table S3 in the Supplement for data citations), accessed through the regridded ETH Zurich CMIP6 archive (Brunner et al., 2020). The emulated FASTMIP-CMIP7 projections and the scripts used to process them and produce the figures are available to referees during review (e.g., through https://github.com/sarasita/fastMIP) and will be made publicly available in a persistent repository with a DOI upon publication; the corresponding link will be included in the final version of the manuscript.

Author contributions. Sa.S. and S.I.S conceptualized the study with input from all authors. Sa.S., M.S., C.B.W., N.S., M.D., S.B., N.M., V.K., D.H., C.S., and R.L. performed the simulations (GCMagicc: N.M.; MESMER: Sa.S.; METEOR: M.S., M.D.; MIT-EarthSampler: C.B.W., S.B.; PRIME: D.H.; RIME-X: N.S., R.L.; SCALES: V.K.; FaIR: M.S., C.S.). J.K. and A.H. supported with IAM data. Sa.S. carried out the formal analysis and visualization with contributions from M.S., C.B.W., N.S., M.D., S.B., and D.H.. Sa.S. wrote the original draft with contributions from M.S., C.B.W., N.S., M.D., and S.B.; all authors reviewed and edited the manuscript.

Competing interests. The authors declare that they have no conflict of interest.

Acknowledgements. We acknowledge the World Climate Research Programme's Coupled Model Intercomparison Project contributors who coordinated and promoted CMIP6. We thank the climate modelling groups for producing and making available their model output, the Earth

https://doi.org/10.5194/egusphere-2026-6328
Preprint. Discussion started: 16 November 2026
© Author(s) 2026. CC BY 4.0 License.

System Grid Federation (ESGF) for archiving the data and providing access, and the multiple funding agencies who support CMIP6 and ESGF.

Sa.S., M.S., M.D., C.S., B.M.S., C.F.S, and S.I.S. received funding from the European Union's Horizon Europe research and innovation programme under grant agreement No 101295156 (FUTURA). Views and opinions expressed are however those of the author(s) only and do not necessarily reflect those of the European Union or the European Climate, Infrastructure and Environment Executive Agency (CINEA). Neither the European Union nor the granting authority can be held responsible for them.

The authors used Claude (Anthropic) to assist with language editing and with converting the manuscript to the Copernicus LaTeX template. All content was written, checked and approved by the authors, who take full responsibility for the manuscript.

https://doi.org/10.5194/egusphere-2026-6328
Preprint. Discussion started: 16 November 2026
© Author(s) 2026. CC BY 4.0 License.

References

Acosta, M. C., Palomas, S., Paronuzzi Ticco, S. V., Utrera, G., Biercamp, J., Bretonniere, P.-A., Budich, R., Castrillo, M., Caubel, A., Doblas-Reyes, F., Epicoco, I., Fladrich, U., Joussaume, S., Kumar Gupta, A., Lawrence, B., Le Sager, P., Lister, G., Moine, M.-P., Rioual, J.-C., Valcke, S., Zadeh, N., and Balaji, V.: The computational and energy cost of simulation and storage for climate science: lessons from CMIP6, Geoscientific Model Development, 17, 3081–3098, https://doi.org/10.5194/gmd-17-3081-2024, 2024.

Bai, H., Liu, X., Yang, H., Chave, J., Ciais, P., Wigneron, J.-P., Saatchi, S., Xiao, J., Le Toan, T., Hu, X., Yang, Z., Wang, L., Fan, L., Yao, Y., Chen, X., Liu, Y., Xue, B., Guo, Q., Tang, Z., Liu, H., Fang, J., and Tao, S.: Unprecedented Amazonian rainforests damage during the 2023–2024 droughts, Proceedings of the National Academy of Sciences, 123, e2514066 123, https://doi.org/10.1073/pnas.2514066123, 2026.

Bauer, V. M., Hauser, M., Quilcaille, Y., Schöngart, S., Gudmundsson, L., and Seneviratne, S. I.: MESMER v1.0.0: consolidating the modular Earth system model emulator into a sustainable research software package, Geoscientific Model Development, 19, 5669–5688, https://doi.org/10.5194/gmd-19-5669-2026, 2026.

Beusch, L., Gudmundsson, L., and Seneviratne, S. I.: Crossbreeding CMIP6 Earth System Models With an Emulator for Regionally Optimized Land Temperature Projections, Geophysical Research Letters, 47, e2019GL086 812, https://doi.org/10.1029/2019GL086812, 2020a.

Beusch, L., Gudmundsson, L., and Seneviratne, S. I.: Emulating Earth system model temperatures with MESMER: from global mean temperature trajectories to grid-point-level realizations on land, Earth System Dynamics, 11, 139–159, https://doi.org/10.5194/esd-11-139-2020, 2020b.

Boardman, P. J. L., Clarke, J., Cox, P. M., Huntingford, C., Jones, C. D., and Williamson, M. S.: Emergent Constraints on Climate Sensitivity and Recent Record-Breaking Warm Years, Earth System Dynamics, 17, 829–841, https://doi.org/10.5194/esd-17-829-2026, 2026.

Bochow, N. and Boers, N.: The South American monsoon approaches a critical transition in response to deforestation, Science Advances, 9, eadd9973, https://doi.org/10.1126/sciadv.add9973, 2023.

Bouabid, S., Souza, A. N., and Ferrari, R.: Score-Based Generative Emulation of Impact-Relevant Earth System Model Outputs, Journal of Advances in Modeling Earth Systems, 18, e2025MS005 558, https://doi.org/10.1029/2025MS005558, 2026.

Boucher, O., Denvil, S., Levavasseur, G., Cozic, A., Caubel, A., Foujols, M.-A., Meurdesoif, Y., Cadule, P., Devilliers, M., Dupont, E., and Lurton, T.: IPSL IPSL-CM6A-LR model output prepared for CMIP6 ScenarioMIP, https://doi.org/10.22033/ESGF/CMIP6.1532, 2019.

Brunner, L., Hauser, M., Lorenz, R., and Beyerle, U.: The ETH Zurich CMIP6 next generation archive: technical documentation, https://doi.org/10.5281/ZENODO.3734128, version Number: v1.0-final, 2020.

Byers, E., Krey, V., Kriegler, E., Riahi, K., Schaeffer, R., Kikstra, J., Lamboll, R., Nicholls, Z., Sandstad, M., Smith, C., van der Wijst, K., Lecocq, F., Portugal-Pereira, J., Saheb, Y., Stromann, A., Winkler, H., Auer, C., Brutschin, E., Lepault, C., Müller-Casseres, E., Gidden, M., Huppmann, D., Kolp, P., Marangoni, G., Werning, M., Calvin, K., Guivarch, C., Hasegawa, T., Peters, G., Steinberger, J., Tavoni, M., van Vuuren, D., Al Khourdajie, A., Forster, P., Lewis, J., Meinshausen, M., Rogelj, J., Samset, B., and Skeie, R.: AR6 Scenarios Database, https://doi.org/10.5281/zenodo.5886912, 2022.

Byers, E., Werning, M., Perrette, M., Schwind, N., Krey, V., Riahi, K., and Schleussner, C.-F.: Fast climate impact emulation for global temperature scenarios with the rapid impact model emulator (RIME), Environmental Research: Climate, 4, 035 011, https://doi.org/10.1088/2752-5295/adee3d, 2025.

https://doi.org/10.5194/egusphere-2026-6328
Preprint. Discussion started: 16 November 2026
© Author(s) 2026. CC BY 4.0 License.

Chini, L., Hurtt, G., Sahajpal, R., Frolking, S., Klein Goldewijk, K., Sitch, S., Ganzenmüller, R., Ma, L., Ott, L., Pongratz, J., and Poulter, B.: Land-use harmonization datasets for annual global carbon budgets, Earth System Science Data, 13, 4175–4189, https://doi.org/10.5194/essd-13-4175-2021, 2021.

Deser, C., Lehner, F., Rodgers, K. B., Ault, T., Delworth, T. L., DiNezio, P. N., Fiore, A., Frankignoul, C., Fyfe, J. C., Horton, D. E., Kay, J. E., Knutti, R., Lovenduski, N. S., Marotzke, J., McKinnon, K. A., Minobe, S., Randerson, J., Screen, J. A., Simpson, I. R., and Ting, M.: Insights from Earth system model initial-condition large ensembles and future prospects, Nature Climate Change, 10, 277–286, https://doi.org/10.1038/s41558-020-0731-2, 2020.

Dunne, J. P., Hewitt, H. T., Arblaster, J. M., Bonou, F., Boucher, O., Cavazos, T., Dingley, B., Durack, P. J., Hassler, B., Juckes, M., Miyakawa, T., Mizielinski, M., Naik, V., Nicholls, Z., O'Rourke, E., Pincus, R., Sanderson, B. M., Simpson, I. R., and Taylor, K. E.: An evolving Coupled Model Intercomparison Project phase 7 (CMIP7) and Fast Track in support of future climate assessment, Geoscientific Model Development, 18, 6671–6700, https://doi.org/10.5194/gmd-18-6671-2025, 2025.

European Union: Directive 2007/60/EC of the European Parliament and of the Council of 23 October 2007 on the assessment and management of flood risks, Official Journal of the European Union, L 288, 27–34, http://europa.eu, 2007.

Fischer, E. M., Beyerle, U., Bloin-Wibe, L., Gessner, C., Humphrey, V., Lehner, F., Pendergrass, A. G., Sippel, S., Zeder, J., and Knutti, R.: Storylines for unprecedented heatwaves based on ensemble boosting, Nature Communications, 14, 4643, https://doi.org/10.1038/s41467-023-40112-4, 2023.

Frieler, K., Lange, S., Schewe, J., Mengel, M., Treu, S., Otto, C., Volkholz, J., Reyer, C. P. O., Heinicke, S., Jones, C., Blanchard, J. L., Harrison, C. S., Petrik, C. M., Eddy, T. D., Ortega-Cisneros, K., Novaglio, C., Heneghan, R., Tittensor, D. P., Maury, O., Büchner, M., Vogt, T., Quesada Chacón, D., Emanuel, K., Lee, C.-Y., Camargo, S. J., Jägermeyr, J., Rabin, S., Klar, J., Vega Del Valle, I. D., Novak, L., Sauer, I. J., Lasslop, G., Chadburn, S., Burke, E., Gallego-Sala, A., Smith, N., Chang, J., Hantson, S., Burton, C., Gädeke, A., Li, F., Gosling, S. N., Müller Schmied, H., Hattermann, F., Hickler, T., Marcé, R., Pierson, D., Thiery, W., Mercado-Bettín, D., Ladwig, R., Ayala-Zamora, A. I., Forrest, M., Bechtold, M., Reinecke, R., De Graaf, I., Kaplan, J. O., Koch, A., and Lengaigne, M.: Scenario set-up and the new CMIP6-based climate-related forcings provided within the third round of the Inter-Sectoral Model Intercomparison Project (ISIMIP3b, group I and II), https://doi.org/10.5194/egusphere-2025-2103, 2025.

Gyuleva, G., Fischer, E., Knutti, R., and Sippel, S.: Recent Temperature and Energy Imbalance Trends Point to Higher Estimates of Future Warming, https://doi.org/10.5194/egusphere-egu26-17120, 2026.

Hauser, M., Bauer, V., Beusch, L., Nicholls, Z., yquilcaille, Nath, S., l pierini, readthedocs assistant, sarasita, and Schwaab, J.: MESMER-group/mesmer: version v1.0.0, https://doi.org/10.5281/ZENODO.20156753, 2026.

Hawkins, E. and Sutton, R.: The Potential to Narrow Uncertainty in Regional Climate Predictions, 90, 1095–1108, https://doi.org/10.1175/2009BAMS2607.1.

Intergovernmental Panel on Climate Change: Scoping of the Seventh Assessment Report (AR7), Tech. Rep. Intergovernmental Panel on Climate Change, https://www.ipcc.ch/meeting-doc/ipcc-62/, 2025.

IPCC: Climate Change 2022: Mitigation of Climate Change. Contribution of Working Group III to the Sixth Assessment Report of the Intergovernmental Panel on Climate Change, Cambridge University Press, Cambridge, UK and New York, NY, USA, https://doi.org/10.1017/9781009157926, type: Book, 2022.

Iturbide, M., Gutiérrez, J. M., Alves, L. M., Bedia, J., Cerezo-Mota, R., Cimadevilla, E., Cofiño, A. S., Di Luca, A., Faria, S. H., Gorodetskaya, I. V., Hauser, M., Herrera, S., Hennessy, K., Hewitt, H. T., Jones, R. G., Krakovska, S., Manzanas, R., Martínez-Castro, D., Narisma, G. T., Nurhati, I. S., Pinto, I., Seneviratne, S. I., Van Den Hurk, B., and Vera, C. S.: An Update of IPCC Climate Reference Regions for

https://doi.org/10.5194/egusphere-2026-6328
Preprint. Discussion started: 16 November 2026
© Author(s) 2026. CC BY 4.0 License.

Subcontinental Analysis of Climate Model Data: Definition and Aggregated Datasets, 12, 2959–2970, https://doi.org/10.5194/essd-12-2959-2020.

J Oliver, H., Shin, M., and Sanders, O.: Cylc: A Workflow Engine for Cycling Systems, Journal of Open Source Software, 3, 737, https://doi.org/10.21105/joss.00737, 2018.

Jones, C. D., Frölicher, T. L., Koven, C., MacDougall, A. H., Matthews, H. D., Zickfeld, K., Rogelj, J., Tokarska, K. B., Gillett, N. P., Ilyina, T., Meinshausen, M., Mengis, N., Séférian, R., Eby, M., and Burger, F. A.: The Zero Emissions Commitment Model Intercomparison Project (ZECMIP) contribution to C4MIP: quantifying committed climate changes following zero carbon emissions, Geoscientific Model Development, 12, 4375–4385, https://doi.org/10.5194/gmd-12-4375-2019, 2019.

Kain, V., Schwind, N., Högner, A., Nauels, A., Möller, T., Hwong, Y.-L., Langer, R., Schoengart, S., Nicholls, Z., Zecchetto, M., and Schleussner, C.-F.: SCALES-MESH v1.0: Cascaded emulation of Earth system models for impact evaluation, https://doi.org/10.5281/ZENODO.23216182, 2026.

Leach, N. J., Jenkins, S., Nicholls, Z., Smith, C. J., Lynch, J., Cain, M., Walsh, T., Wu, B., Tsutsui, J., and Allen, M. R.: FaIRv2.0.0: a generalized impulse response model for climate uncertainty and future scenario exploration, Geoscientific Model Development, 14, 3007–3036, https://doi.org/10.5194/gmd-14-3007-2021, 2021.

Lee, J.-Y., Marotzke, J., Bala, G., Cao, L., Corti, S., Dunne, J., Engelbrecht, F., Fischer, E., Fyfe, J., Jones, C., Maycock, A., Mutemi, J., Ndiaye, O., Panickal, S., and Zhou, T.: Future Global Climate: Scenario-Based Projections and Near-Term Information, in: Climate Change 2021: The Physical Science Basis. Contribution of Working Group I to the Sixth Assessment Report of the Intergovernmental Panel on Climate Change, edited by Masson-Delmotte, V., Zhai, P., Pirani, A., Connors, S. L., Péan, C., Berger, S., Caud, N., Chen, Y., Goldfarb, L., Gomis, M. I., Huang, M., Leitzell, K., Lonnoy, E., Matthews, J. B. R., Maycock, T. K., Waterfield, T., Yelekçi, O., Yu, R., and Zhou, B., pp. 553–672, Cambridge University Press, Cambridge, UK and New York, NY, USA, https://doi.org/10.1017/9781009157896.006, section: 4 Type: Book Section, 2021.

Lehner, F., Deser, C., Maher, N., Marotzke, J., Fischer, E. M., Brunner, L., Knutti, R., and Hawkins, E.: Partitioning Climate Projection Uncertainty with Multiple Large Ensembles and CMIP5/6, 11, 491–508, https://doi.org/10.5194/esd-11-491-2020.

Mankin, J. S., Lehner, F., Coats, S., and McKinnon, K. A.: The Value of Initial Condition Large Ensembles to Robust Adaptation Decision-Making, Earth's Future, 8, e2012EF001 610, https://doi.org/10.1029/2020EF001610, 2020.

Mathison, C., Burke, E. J., Munday, G., Jones, C. D., Smith, C. J., Steinert, N. J., Wiltshire, A. J., Huntingford, C., Kovacs, E., Gohar, L. K., Varney, R. M., and McNeall, D.: A rapid-application emissions-to-impacts tool for scenario assessment: Probabilistic Regional Impacts from Model patterns and Emissions (PRIME), Geoscientific Model Development, 18, 1785–1808, https://doi.org/10.5194/gmd-18-1785-2025, 2025.

Meinshausen, N., Meinshausen, M., Lewis, J., Nicholls, Z., Schöngart, S., Self, A., Shen, X., Spiller, K., and Vogel, E.: GCMagicc v1: a fast generative emulator for multivariate climate-impact ensembles, https://doi.org/10.48550/arXiv.2609.08383, arXiv:2609.08383 [physics.ao-ph], 2026a.

Meinshausen, N., Meinshausen, M., Lewis, J., Nicholls, Z., Schöngart, S., Self, A., Shen, X., Spiller, K., and Vogel, E.: Trained model checkpoints and validation data for "GCMagicc v1: a fast generative emulator for multivariate climate-impact ensembles", https://doi.org/10.5281/ZENODO.22139683, 2026b.

Milinski, S., Maher, N., and Olonscheck, D.: How large does a large ensemble need to be?, Earth System Dynamics, 11, 885–901, https://doi.org/10.5194/esd-11-885-2020, 2020.

https://doi.org/10.5194/egusphere-2026-6328
Preprint. Discussion started: 16 November 2026
© Author(s) 2026. CC BY 4.0 License.

Nath, S., Lejeune, Q., Beusch, L., Seneviratne, S. I., and Schleussner, C.-F.: MESMER-M: an Earth system model emulator for spatially resolved monthly temperature, Earth System Dynamics, 13, 851–877, https://doi.org/10.5194/esd-13-851-2022, 2022.

O'Neill, B. C., Tebaldi, C., Van Vuuren, D. P., Eyring, V., Friedlingstein, P., Hurtt, G., Knutti, R., Kriegler, E., Lamarque, J.-F., Lowe, J., Meehl, G. A., Moss, R., Riahi, K., and Sanderson, B. M.: The Scenario Model Intercomparison Project (ScenarioMIP) for CMIP6, Geoscientific Model Development, 9, 3461–3482, https://doi.org/10.5194/gmd-9-3461-2016, 2016.

Pirani, A., Fuglestvedt, J. S., Byers, E., O'Neill, B., Riahi, K., Lee, J.-Y., Marotzke, J., Rose, S. K., Schaeffer, R., and Tebaldi, C.: Scenarios in IPCC assessments: lessons from AR6 and opportunities for AR7, npj Climate Action, 3, 1, https://doi.org/10.1038/s44168-023-00082-1, 2024.

Quilcaille, Y., Gudmundsson, L., and Seneviratne, S. I.: Extending MESMER-X: a spatially resolved Earth system model emulator for fire weather and soil moisture, Earth System Dynamics, 14, 1333–1362, https://doi.org/10.5194/esd-14-1333-2023, 2023.

Quilcaille, Y., Bauer, V., Hauser, M., Schöngart, S., Gudmundsson, L., and Seneviratne, S. I.: Parametrizations for MESMER v1.0.0, https://doi.org/10.3929/ETHZ-C-000798034, 2026.

Rawshan Ara Begum, R., Lempert, R., E. Ali, T. B., Bernauer, T., Cramer, W., Cui, X., Mach, K., Nagy, G., Stenseth, N., Sukumar, R., and Wester, P.: Point of Departure and Key Concepts, in: Climate Change 2022: Impacts, Adaptation and Vulnerability. Contribution of Working Group II to the Sixth Assessment Report of the Intergovernmental Panel on Climate Change, edited by Pörtner, H. O., Roberts, D. C., Tignor, M., Poloczanska, E. S., Mintenbeck, K., Alegría, A., Craig, M., Langsdorf, S., Löschke, S., Möller, V., Okem, A., and Rama, B., Cambridge University Press, Cambridge, UK and New York, NY, USA, https://doi.org/10.1017/9781009325844.003, section: 1 Type: Book Section, 2022.

Riahi, K., Schaeffer, R., Arango, J., Calvin, K., Guivarch, C., Hasegawa, T., Jiang, K., Kriegler, E., Matthews, R., Peters, G., Rao, A., Robertson, S., Sebbit, A., Steinberger, J., Tavoni, M., and Van Vuuren, D.: Mitigation pathways compatible with long-term goals, in: Climate Change 2022: Mitigation of Climate Change. Contribution of Working Group III to the Sixth Assessment Report of the Intergovernmental Panel on Climate Change, edited by Shukla, P., Skea, J., Slade, R., Khourdajie, A. A., van Diemen, R., McCollum, D., Pathak, M., Some, S., Vyas, P., Fradera, R., Belkacemi, M., Hasija, A., Lisboa, G., Luz, S., and Malley, J., Cambridge University Press, Cambridge, UK and New York, NY, USA, https://doi.org/10.1017/9781009157926.005, section: 3 Type: Book Section, 2022.

Sanderson, B., Sandstad, M., Brovkin, V., Fisher, R., Hohn, D., Ilyina, T., Jones, C., Koenigk, T., Koven, C., Li, H., Lawrence, D., Lawrence, P., Liddicoat, S., MacDougall, A. H., Mengis, N., Nicholls, Z., O'Rourke, E., Romanou, A., Schwinger, J., Séférian, R., Sentman, L. T., Simpson, I. R., Smith, C., Steinert, N. J., Swann, A. L. S., Tjiputra, J., and Ziehn, T.: flat10-MIP, https://doi.org/10.11582/2026.DQDLGH8G, artwork Size: 4802 kb Pages: 4802 kb, 2026a.

Sanderson, B. M., Sandstad, M., Dewey, M., Steinert, N. J., and Fjeldså, J. L.: METEORv1.6: Spatial climate variability and integrated impact emulation, https://doi.org/10.5194/egusphere-2026-2029, 2026b.

Sandstad, M., Steinert, N. J., Baur, S., and Sanderson, B. M.: METEORv1.0.1: a novel framework for emulating multi-timescale regional climate responses, Geoscientific Model Development, 18, 8269–8312, https://doi.org/10.5194/gmd-18-8269-2025, 2025.

Schleussner, C.-F., Ganti, G., Lejeune, Q., Zhu, B., Pfleiderer, P., Prütz, R., Ciais, P., Frölicher, T. L., Fuss, S., Gasser, T., Gidden, M. J., Kropf, C. M., Lacroix, F., Lamboll, R., Martyr, R., Maussion, F., McCaughey, J. W., Meinshausen, M., Mengel, M., Nicholls, Z., Quilcaille, Y., Sanderson, B., Seneviratne, S. I., Sillmann, J., Smith, C. J., Steinert, N. J., Theokritoff, E., Warren, R., Price, J., and Rogelj, J.: Overconfidence in Climate Overshoot, 634, 366–373, https://doi.org/10.1038/s41586-024-08020-9.

Schoengart, S., Gudmunsson, L., Womack, C. B., Schleussner, C.-F., and Seneviratne, S. I.: A Review of Spatially Explicit Climate Emulators as Agile Tools for Decision-Support, https://doi.org/10.21203/rs.3.rs-11205768/v1, 2026.

https://doi.org/10.5194/egusphere-2026-6328
Preprint. Discussion started: 16 November 2026
© Author(s) 2026. CC BY 4.0 License.

Schupfner, M., Wieners, K.-H., Wachsmann, F., Milinski, S., Steger, C., Bittner, M., Jungclaus, J., Früh, B., Pankatz, K., Giorgetta, M., Reick, C., Legutke, S., Esch, M., Gayler, V., Haak, H., de Vrese, P., Raddatz, T., Mauritsen, T., von Storch, J.-S., Behrens, J., Brovkin, V., Claussen, M., Crueger, T., Fast, I., Fiedler, S., Hagemann, S., Hohenegger, C., Jahns, T., Kloster, S., Kinne, S., Lasslop, G., Kornblueh, L., Marotzke, J., Matei, D., Meraner, K., Mikolajewicz, U., Modali, K., Müller, W., Nabel, J., Notz, D., Peters-von Gehlen, K., Pincus, R., Pohlmann, H., Pongratz, J., Rast, S., Schmidt, H., Schnur, R., Schulzweida, U., Six, K., Stevens, B., Voigt, A., and Roeckner, E.: DKRZ MPI-ESM1.2-LR model output prepared for CMIP6 ScenarioMIP, https://doi.org/10.22033/ESGF/CMIP6.15349, 2021.

Schwaab, J., Hauser, M., Lamboll, R. D., Beusch, L., Gudmundsson, L., Quilcaille, Y., Lejeune, Q., Schöngart, S., Schleussner, C.-F., Nath, S., and others: Spatially resolved emulated annual temperature projections for overshoot pathways, Scientific Data, 11, 1262, https://doi.org/10.1038/s41597-024-04122-1, 2024.

Schwind, N., Perrette, M., Byers, E., Högner, A., Lejeune, Q., Möller, T., Nicholls, Z., Pfleiderer, P., Schöngart, S., Werning, M., and Schleussner, C.-F.: RIME-X v1.0: Combining Simple Climate Models, Earth System Models, and Climate Impact Models into a Unified Statistical Emulator for Regional Climate Indicators, https://doi.org/10.5194/egusphere-2025-5781, 2026a.

Schwind, N., Perrette, M., Byers, E., Högner, A., Lejeune, Q., Möller, T., Nicholls, Z., Schoengart, S., Pfleiderer, P., Werning, M., and Schleussner, C.-F.: Code and Data for Paper: "RIME-X v1.0: Combining Simple Climate Models, Earth System Models, and Climate Impact Models into a Unified Statistical Emulator for Regional Climate Indicators", https://doi.org/10.5281/ZENODO.17491734, language: en, 2026b.

Schöngart, S., Gudmundsson, L., Hauser, M., Pfleiderer, P., Lejeune, Q., Nath, S., Seneviratne, S. I., and Schleußner, C.-F.: Introducing the MESMER-M-TPv0.1.0 module: Spatially Explicit Earth System Model Emulation for Monthly Precipitation and Temperature, EGUsphere, 2024, 1–51, https://doi.org/10.5194/egusphere-2024-278, 2024.

Serreze, M. C. and Barry, R. G.: Processes and impacts of Arctic amplification: A research synthesis, Global and Planetary Change, 77, 85–96, https://doi.org/10.1016/j.gloplacha.2011.03.004, 2011.

Shepherd, T. G.: Atmospheric circulation as a source of uncertainty in climate change projections, Nature Geoscience, 7, 703–708, https://doi.org/10.1038/ngeo2253, 2014.

Shin, M., Fitzpatrick, B., Clark, A., Sanders, O., Pillinger, T., Dutta, R., Bartholomew, S. L., Whitehouse, S., Matthews, D., Oxley, S., Trzeciak, T., Valters, D., Oliver, H. J., Mancell, J., Hall, M., Coleman, T., Shepherd, H., Osprey, A., Seddon, J., Theodorakis, D., Joe, J-J-Abram, Dix, M., Sharp, R., metofcm, Frost, J., Dawson, M., and Cresswell, P.: metomi/rose: Rose 2.3.2, https://doi.org/10.5281/ZENODO.14096377, 2024.

Smith, C.: fair calibration data, https://doi.org/10.5281/ZENODO.18828694, 2026.

Smith, C., Cummins, D. P., Fredriksen, H.-B., Nicholls, Z., Meinshausen, M., Allen, M., Jenkins, S., Leach, N., Mathison, C., and Partanen, A.-I.: fair-calibrate v1.4.1: calibration, constraining, and validation of the FaIR simple climate model for reliable future climate projections, Geoscientific Model Development, 17, 8569–8592, https://doi.org/10.5194/gmd-17-8569-2024, 2024.

Sutton, R. T., Dong, B., and Gregory, J. M.: Land/sea warming ratio in response to climate change: IPCC AR4 model results and comparison with observations, Geophysical Research Letters, 34, 2006GL028 164, https://doi.org/10.1029/2006GL028164, 2007.

Swaminathan, R., Schewe, J., Walton, J., Zimmermann, K., Jones, C., Betts, R. A., Burton, C., Jones, C. D., Mengel, M., Reyer, C. P. O., Turner, A. G., and Weigel, K.: Regional Impacts Poorly Constrained by Climate Sensitivity, Earth's Future, 12, e2024EF004 901, https://doi.org/10.1029/2024EF004901, 2024.

https://doi.org/10.5194/egusphere-2026-6328
Preprint. Discussion started: 16 November 2026
© Author(s) 2026. CC BY 4.0 License.

Swart, N. C., Cole, J. N., Kharin, V. V., Lazare, M., Scinocca, J. F., Gillett, N. P., Anstey, J., Arora, V., Christian, J. R., Jiao, Y., Lee, W. G., Majaess, F., Saenko, O. A., Seiler, C., Seinen, C., Shao, A., Solheim, L., von Salzen, K., Yang, D., Winter, B., and Sigmond, M.: CCCma CanESM5 model output prepared for CMIP6 ScenarioMIP, https://doi.org/10.22033/ESGF/CMIP6.1317, 2019.

Tatebe, H. and Watanabe, M.: MIROC MIROC6 model output prepared for CMIP6 CMIP, https://doi.org/10.22033/ESGF/CMIP6.881, 2018.

Tebaldi, C. and Knutti, R.: The use of the multi-model ensemble in probabilistic climate projections, Philosophical Transactions of the Royal Society A: Mathematical, Physical and Engineering Sciences, 365, 2053–2075, https://doi.org/10.1098/rsta.2007.2076, 2007.

Tebaldi, C., Debeire, K., Eyring, V., Fischer, E., Fyfe, J., Friedlingstein, P., Knutti, R., Lowe, J., O'Neill, B., Sanderson, B., Van Vuuren, D., Riahi, K., Meinshausen, M., Nicholls, Z., Tokarska, K. B., Hurtt, G., Kriegler, E., Lamarque, J.-F., Meehl, G., Moss, R., Bauer, S. E., Boucher, O., Brovkin, V., Byun, Y.-H., Dix, M., Gualdi, S., Guo, H., John, J. G., Kharin, S., Kim, Y., Koshiro, T., Ma, L., Olivié, D., Panickal, S., Qiao, F., Rong, X., Rosenbloom, N., Schupfner, M., Séférian, R., Sellar, A., Semmler, T., Shi, X., Song, Z., Steger, C., Stouffer, R., Swart, N., Tachiiri, K., Tang, Q., Tatebe, H., Voldoire, A., Volodin, E., Wyser, K., Xin, X., Yang, S., Yu, Y., and Ziehn, T.: Climate model projections from the Scenario Model Intercomparison Project (ScenarioMIP) of CMIP6, Earth System Dynamics, 12, 253–293, https://doi.org/10.5194/esd-12-253-2021, 2021.

Tebaldi, C., Selin, N., Ferrari, R., and Flierl, G.: Emulators of Climate Model Output, Annual Review of Environment and Resources, https://doi.org/10.1146/annurev-environ-012125-085838, 2025.

Thompson, V., Dunstone, N. J., Scaife, A. A., Smith, D. M., Slingo, J. M., Brown, S., and Belcher, S. E.: High risk of unprecedented UK rainfall in the current climate, Nature Communications, 8, 107, https://doi.org/10.1038/s41467-017-00275-3, 2017.

UNFCCC: Paris Agreement, https://unfccc.int/process/conferences/pastconferences/paris-climate-change-conference-november-2015/paris-agreement.

Van Vuuren, D. P., O'Neill, B. C., Tebaldi, C., Sanderson, B. M., Chini, L. P., Friedlingstein, P., Hasegawa, T., Riahi, K., Govindasamy, B., Bauer, N., Eyring, V., Fall, C. M. N., Frieler, K., Gidden, M. J., Gohar, L. K., Högner, A., Jones, A. D., Kikstra, J., King, A., Knutti, R., Kriegler, E., Lawrence, P., Lennard, C., Lowe, J., Mathison, C., Mehmood, S., Nicholls, Z., Prado, L. F., Zhang, Q., Rose, S. K., Ruane, A. C., Sandstad, M., Schleussner, C.-F., Seferian, R., Sillmann, J., Smith, C., Sörensson, A. A., Panickal, S., Tachiiri, K., Vaughan, N., Vishwanathan, S. S., Yokohata, T., Zecchetto, M., and Ziehn, T.: The Scenario Model Intercomparison Project for CMIP7 (ScenarioMIP-CMIP7), Geoscientific Model Development, 19, 2627–2656, https://doi.org/10.5194/gmd-19-2627-2026, 2026.

Windisch, M. G., Quilcaille, Y., Mathison, C., Tebaldi, C., Burke, E., Gohar, L., Smith, C., Schöngart, S., Snyder, A., Durga, S., Dorheim, K., and Seneviratne, S.: Advancing the scenario-to-climate link with spatial emulators in the FASTMIP pilot experiment, https://doi.org/10.5194/egusphere-2026-2253, 2026.

Ziehn, T., Chamberlain, M., Lenton, A., Law, R., Bodman, R., Dix, M., Wang, Y., Dobrohotoff, P., Srbinovsky, J., Stevens, L., Vohralik, P., Mackallah, C., Sullivan, A., O'Farrell, S., and Druken, K.: CSIRO ACCESS-ESM1.5 model output prepared for CMIP6 ScenarioMIP, https://doi.org/10.22033/ESGF/CMIP6.2291, 2019.